UNIVERSITÀ DEGLI STUDI DI BRESCIA

DIPARTIMENTO DI MEDICINA MOLECOLARE E TRASLAZIONALE (DMMT)

DOTTORATO DI RICERCA IN GENETICA MOLECOLARE, BIOTECNOLOGIE E MEDICINA SPERIMENTALE (- D.M. 45/2013)

Settore Scientifico Disciplinare: BIOs12AU

CICLO: XXXVII

From flat to spatial: transitioning from 2D to 3D in vitro models for Nicotine based oxidative Stress and lung granuloma formation

(Dalla bidimensionalità alla tridimensionalità: transizione dalle colture classiche 2D ai modelli avanzati 3D per l'analisi dello stress ossidativo indotto dalla nicotina nel contesto della formazione di granulomi polmonari)

SUPERVISORE DI TESI

Chiar.ma Prof.ssa Rita Rezzani

Co- SUPERVISORE DI TESI

Chiar.ma Prof.ssa Daniela Maria Cirillo

COORDINATORE

Chiar.mo Prof. Eugenio Monti

DOTTORANDO

Dott.ssa Franco Caterina

Anno Accademico 2024/2025

Blank page

FIRST PAGE

"It takes one step to start a journey
It's up to you to make it real."

A chi, in questi tre anni,

mi ha ricordato di respirare.

Table of Contents

Abstract (English Version)

Tuberculosis remains one of the leading causes of mortality worldwide. It is caused by *Mycobacterium tuberculosis*. The infection typically begins in the lungs, where bronchial epithelial cells serve as the first line of defense against the pathogen. The immune response in the lungs leads to the formation of granulomas, structured cellular aggregates designed to contain the pathogen. However, the pulmonary microenvironment is frequently exposed to oxidative stress conditions, which can increase cell susceptibility to infection. Despite extensive research using animal models and bidimensional (2D) cellular systems, these models often fail to replicate lung tissue's cellular interactions and physiological conditions accurately.

This thesis focuses on developing a three-dimensional (3D) bioprinted lung model to mimic a tubercular granuloma. The aim is to better understand how the lung microenvironment, particularly in the presence of oxidative stress-inducing molecules such as nicotine (commonly associated with smokers), influences the establishment of *Mycobacterium tuberculosis* infection and subsequent granuloma formation.

In this study, three cell types were employed: human bronchial epithelial cells (HBEC3-KT) for the epithelial barrier, human leukemia monocytic cell line (THP-1) differentiated into macrophages to represent the immune component, and human lung fibroblasts (HLF hTERT) to provide connective tissue support. Infections were conducted using a *Mycobacterium tuberculosis* reference strain H37Rv (mCHERRY+) fluorescent mutant. Oxidative stress conditions were optimized using 2D experiments, and a nicotine concentration of 40 μM was selected as the final exposure condition.

Cell viability was evaluated using Alamar Blue assays for 2D cultures and Live/Dead staining for 3D cultures, while bacterial load was quantified using colony-forming unit counts. The results demonstrated that *Mycobacterium tuberculosis* is more prone to infect the granuloma-like structures designed in the study when pre-treated with nicotine.

This innovative 3D model offers a physiologically relevant platform to study the molecular dynamics between lung cells and *Mycobacterium tuberculosis* during the early infection and granuloma formation stages. Furthermore, it addresses limitations associated with 2D cultures by enabling the exploration of oxidative stress-inducing molecules, such as nicotine, in a fully humanized and dynamic model.

Abstract (Italian Version)

La tubercolosi è una delle principali cause di mortalità a livello globale ed è causata da *Mycobacterium tuberculosis*. L'infezione inizia tipicamente nei polmoni, dove le cellule epiteliali bronchiali rappresentano la prima linea di difesa locale contro il patogeno. La risposta immunitaria polmonare porta alla formazione di granulomi, aggregati cellulari strutturati volti a contenere il microrganismo. Tuttavia, il microambiente polmonare è frequentemente esposto a condizioni di stress ossidativo, che possono aumentare la suscettibilità cellulare all'infezione. Nonostante i numerosi studi condotti su modelli animali e sistemi cellulari bidimensionali (2D), questi modelli spesso non riescono a replicare accuratamente le interazioni cellulari e le condizioni fisiologiche del tessuto polmonare.

Questa tesi si concentra sullo sviluppo di un modello polmonare tridimensionale sviluppato tramite un sistema di bioprinting che ha come scopo finale quello di simulare un granuloma tubercolare, al fine di approfondire la comprensione di come il microambiente polmonare, in particolare in presenza di molecole che inducono stress ossidativo come la nicotina, influenzi l'instaurarsi dell'infezione da *Mycobacterium tuberculosis* e la successiva formazione del granuloma.

Nello studio sono stati utilizzati tre tipi cellulari: cellule epiteliali bronchiali umane (HBEC3-KT) per la barriera epiteliale, cellule monocitiche umane derivate dalla linea cellulare leucemica (THP-1) differenziate in macrofagi per rappresentare la componente immunitaria, e fibroblasti polmonari umani (HLF hTERT) per ricreare il supporto connettivale. Le infezioni sono state condotte utilizzando un mutante fluorescente del ceppo di riferimento Mtb

H37Rv (mCHERRY+). Le condizioni di stress ossidativo sono state ottimizzate attraverso esperimenti in 2D, selezionando una concentrazione finale di nicotina pari a 40 μM.

La vitalità cellulare è stata valutata tramite saggi Alamar Blue per le colture 2D e colorazioni Live/Dead per le colture 3D, mentre il carico batterico è stato quantificato mediante conteggio delle unità formanti colonie. I risultati hanno dimostrato che *Mycobacterium tuberculosis* ha una maggiore propensione a infettare le strutture simili a granulomi progettate nello studio dopo pre-trattamento con nicotina.

Questo modello 3D innovativo offre una piattaforma fisiologicamente rilevante per studiare le dinamiche molecolari tra le cellule polmonari e Mycobacterium tuberculosis durante le fasi iniziali dell'infezione e della formazione del granuloma. Inoltre, affronta le limitazioni dei modelli 2D, consentendo l'esplorazione di molecole che inducono stress ossidativo, come la nicotina, in un sistema completamente umanizzato e dinamico.

Introduction

The lung is a complex organ in which it is possible to find more than 50 cell types with different origins. These cells are distributed across different lung compartments, such as airways, blood and lymphatic vessels, connective tissue, nerves, mesothelium, and lung parenchyma. Moreover, they are exposed to various stimuli, highlighting the high complexity of lung organization [1].

Respiratory infections are prevalent worldwide and were already rising before the COVID-19 pandemic, leading to significant morbidity and mortality. They rank as the third-leading cause of premature death and are linked to many chronic respiratory conditions [2]. Moreover, recent studies have demonstrated the involvement of respiratory infections, both viral and bacterial, in the development and progression of lung cancer.

For this reason, understanding how respiratory infectious diseases behave in models that mimic physiological lung conditions is essential for developing effective vaccines and treatments [3].

Among all the pulmonary infectious pathogens, *Mycobacterium tuberculosis* (Mtb), the bacteria responsible for Tuberculosis (TB), is one of the two leading causes of infectious death worldwide [4].

TB is one of the oldest acquired infectious diseases, constituting a persistent threat to public health. Designated as a Global Emergency by the World Health Organization (WHO) in 1993, it has infected approximately 10.6 million individuals worldwide and caused 1.3 million deaths, making it one of the primary causes of mortality attributed to a single infectious agent. Additionally, an estimated one-fourth of the global population (~1.7 billion people) carries latent tuberculosis infection (LTBI) [5].

It's important to note that Mtb can adapt to the human host continuously, and this specific feature adds another layer of complexity to TB management alongside the emergence of drug-resistant strains.

Thus, developing new models to study Mtb infection, from the initial stages through granuloma formation, is essential for advancing our understanding of TB and improving treatment and prevention strategies. This study represents a groundbreaking application of 3D bioprinted models, substantially improving over traditional 2D and animal-based methods. Simulating the structural and functional dynamics of the pulmonary microenvironment provides a novel and more physiologically relevant approach to understanding TB pathogenesis and treatment development. Current models, particularly animal and in vitro systems, provide limited insight due to significant differences between human and model immune responses, especially in granuloma formation, where human-specific immune processes play a critical role [6]. The application of 3D bioprinted models marks a transformative step in tuberculosis research, offering capabilities that surpass traditional 2D cultures and animal models. Unlike 2D systems, which fail to replicate the spatial architecture and dynamic cell-cell interactions of lung tissue, 3D bioprinted models recreate the pulmonary microenvironment with high fidelity.

Additionally, while animal models provide valuable insights, they are often limited by interspecies differences in immune responses and granuloma formation. The 3D bioprinted model employed in this study not only incorporates human-relevant cells but also allows precise control over experimental conditions, enabling the study of host-pathogen interactions and oxidative stress in a manner that is both physiologically relevant and ethically favorable. This innovative approach sets a new standard for studying

tuberculosis pathogenesis, granuloma formation, and the impact of external factors such as nicotine exposure.

Granulomas, organized structures formed by immune cells to contain the infection, involve complex host-pathogen interactions, including a balance between immune containment and tissue damage, which is difficult to replicate outside of human systems [6]. Traditional models often do not capture this dynamic or support long-term studies that simulate the months or years over which TB progresses in humans [7].

New approaches are emerging, such as 3D in vitro culture models using human cells to closely approximate granuloma structures and lung organoid and organ-on-chip models that mimic human lung architecture and physiological conditions [8]. Humanized animal models with human immune cells offer more accurate reflections of the immune response to TB and show promise in understanding granuloma dynamics and immune interactions [9]. Combined with advanced imaging and computational techniques, these models allow for real-time visualization and analysis of granuloma development and can simulate various aspects of TB pathogenesis under controlled conditions [10].

Developing new models will accelerate the discovery of effective therapies and vaccines, improve our understanding of TB progression, and enable the identification of novel therapeutic targets, all of which are critical to addressing the global TB epidemic.

Furthermore, there is an urgent need for rapid and accurate diagnostic tools to control TB transmission.

These models are particularly critical if we consider that a lot remains to be defined in the complex dynamics of TB infection. The development of new physiologic three-dimensional models has the potential to recreate a more

accurate representation of the pulmonary microenvironment, including the interactions between epithelial cells, immune cells, and pathogens.

This possibility acquires even more importance if we consider the critical burden of what is nowadays recognized as a sort of "epidemic": the cigarette smoking (CS) exposure [11].

Data have largely confirmed that both primary and secondary exposure to the CS components, in particular to the nicotine, can compromise epithelial barrier integrity and alter immune responses, further complicating TB progression.

Nicotine (Nic) is one of the key components of the CS. It can affect the tight junctions (TJ) in bronchial epithelial cells, disrupting the barrier integrity, increasing lung permeability, and facilitating pathogen invasion [12].

This disruption enhances susceptibility to pathogen infection and exacerbates inflammation, contributing to a more favorable bacterial growth and dissemination environment. Existing studies have shown that nicotine has a profound impact on immune cell function during Mtb infection [13]. Specifically, it has been shown to alter the activation of key immune cells, such as macrophages and T cells, impairing their ability to mount an effective immune response. This immunosuppressive effect not only hinders the initial defense against Mtb but also affects granuloma formation. In addition, nicotine exposure leads to an increase in oxidative stress and to an alteration in cytokine production, further exacerbating the inflammatory environment and promoting Mtb persistence[14].

Understanding how nicotine enters these critical cellular interactions is essential for developing targeted interventions and improving therapeutic strategies, particularly for individuals with a history of smoking or exposure to nicotine products.

By integrating these insights into advanced three-dimensional models, we can better understand the nicotine's effects on pulmonary defenses and accelerate the development of more effective treatment approaches.

In the end, to effectively combat the growing burden of TB, it is crucial to implement robust prevention strategies that address both the environmental factors, such as nicotine exposure, and the biological mechanisms underlying the disease. This will enhance the effectiveness of public health interventions and reduce the incidence of TB worldwide.

Chapter 1: Lung Anatomy and Tuberculosis Pathogenesis: Exploring Immune Responses and Structural Models

Lung architecture and physiological structure

Lungs are paired, symmetrical organs that are part of the respiratory system. They are located within the chest in the two pleural cavities, laterally to the mediastinum.

The lung bud appears on the 26th day of gestation as an outgrowth of the primitive gut. It comprises undifferentiated epithelial cells that expand into the surrounding embryonic connective tissue or mesenchyme. The development of the functional component of the lungs, the alveoli, begins later: the alveolar phase starts almost at the end of gestation, around the 36th week, continuing into early childhood, around 18-24 months of age, resulting in the formation of a final number of alveoli estimated at around 200-300 million [15].

In an adult subject, lungs can be defined as sophisticated organs comprised of semi-rigid conducting tubes branching and narrowing from the trachea, bronchi, and bronchioles, ultimately leading to highly vascularized sacs known as alveoli, where respiratory gases are exchanged.

These airways consist of various cell types, primarily from the embryonic neuroectoderm, mesoderm, and endoderm. Within the mature lung, different types of cells exist in specific proportions and locations, forming the structural elements crucial for ventilation. This intricate structure is shaped by continuous exposure to particles, pathogens, and toxicants through the secretion of protective mucus and surfactants, active mucociliary clearance, and an essential innate and acquired immune system [16].

The conducting airways in the lungs are primarily populated by four main types of epithelial cells: ciliated cells, goblet cells, and basal cells.

Ciliated cells facilitate mucus movement through synchronous cilia beating, while goblet cells secrete mucus onto airway surfaces. Basal cells act as adult stem cells, predominantly lining larger airways [17].

Other sparse cell populations include club cells, which produce lubricating substances and antimicrobial peptides, and pulmonary neuroendocrine cells, which release proteins under physiological stimuli like hypoxia. Less common cell types include ionocytes and brush cells [16] (Figure 1).

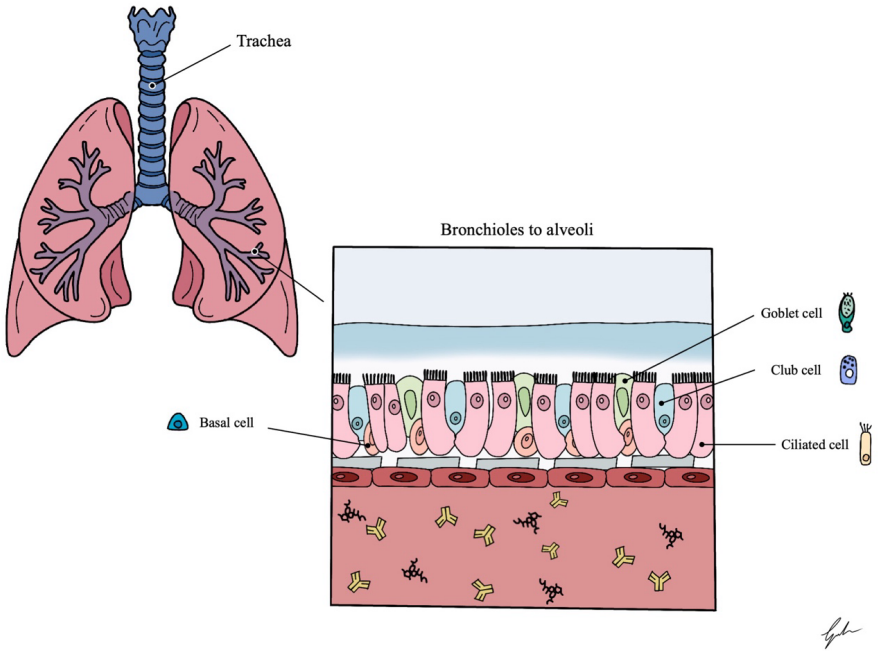

Figure 1. Schematic representation of the main cell lines that are present in the lung. It highlights the different compositions of the innermost epithelial compartment in the various portions of the respiratory tract. Adapted from Dichtl et al., "The breathtaking world of human respiratory in vitro models: Investigating lung diseases and infections in 3D models, organoids, and lung-on-chip" Eur.J.Immuno, 2024, published under the terms of the Creative Commons Attribution License (CC BY) [18].

The respiratory tract and lungs perform several vital functions in the body. They are essential in facilitating respiration, supporting pulmonary circulation, and contributing to the immune system.

Considering the complexity of this system, reliable physiological and pathological models are essential to enhancing our understanding of the mechanisms and pathomechanisms in the respiratory tract and lungs [18].

Tubercular infection

TB, caused by the microorganism belonging to the *Mycobacterium tuberculosis complex* (MTBC), is a preventable infectious disease that typically enters the body through the respiratory tract, primarily targeting the lungs.

TB is transmitted via aerosol droplets with dimensions ranging from 1 to 5 μm. It affects 10 million people worldwide each year, and it is one of the infectious diseases with higher mortality rates. It is the world's second leading cause of death from a single infectious agent [4,20]

The human-adapted Mtb is well known for its adaptability to the host immune system, allowing it to persist within the infected host. For this reason, TB eradication typically requires 6 to 9 months of multidrug chemotherapy, making it a complicated task [21].

Moreover, multidrug-resistant or rifampicin-resistant TB (MDR/RR-TB) presents a growing public health challenge in many regions, particularly in Eastern Europe, Russia, Asia, and sub-Saharan Africa.

Considering what has been said before, immediate and rapid action is necessary to eliminate what is recognized as a global "TB epidemic" by 2030, a target endorsed by all United Nations (UN) Member States and the WHO [22].

Patients infected with Mtb can develop a wide array of symptoms and manifestations [23]. Traditionally, the Mtb infection has been described through

a dichotomy: LTBI, which is asymptomatic, and 'active' TB disease (ATB), which is contagious and symptomatic. Recent advancements in understanding TB pathogenesis highlighted that the step that takes us from Mtb infection to the Tubercular disease is a more complex continuum identifying eight broad conceptual themes to categorize TB states, summarized in Figure 2 [24].

Stage	Categorical state	Previous *Mtb* exposure	Viable *Mtb* detectable	Radiographic abnormalities		
STAGE 0	UNINFECTED	yes	no	no	Infection has been eliminated with innate immune response	
STAGE 1	LTBI **ASYMPTOMATIC**	yes	yes	no	Infection has been eliminated by the acquired immune response	Diagnosed through TB skin tests or blood tests (IGRAS)
STAGE 2	QUIESCENT INFECTION **ASYMPTOMATIC**	yes	yes	no	Infection is not eradicated but is controlled by the immune system	Difficult to diagnose
STAGE 3	INCIPIENT TB **ASYMPTOMATIC**	yes	yes	no	Infection is not controlled by the immune system	Difficult to diagnose
STAGE 4	SUBCLINICAL TB **ASYMPTOMATIC**	yes	yes	yes	Individual is bacteriologically positive but exhibits no symptoms or clinical features	Difficult to diagnose: multipicity of tests
STAGE 5	CLINICAL TB **SYMPTOMATIC**	yes	yes	yes	Individual exhibits signs or symptoms associated with TB	Diagnosed through sputum culture, chest X-ray, molecular tests, and clinical evaluation
STAGE 6	CAVITARY/ DISSEMINATED TB **SYMPTOMATIC**	yes	yes	yes	High severity of disease due to clinical features, radiology, or bacteriology	Diagnosed through sputum culture, chest X-ray, molecular tests, and clinical evaluation
STAGE 7	PAST TB (TREATED/ RECOVERED) **SYMPTOMATIC**	yes	no	yes/no	Previous History of TB	Clinical evaluation, medical history

Figure 2. Schematic representation of the spectrum of TB disease.

This distinction is particularly relevant because it clarifies that a symptom-driven approach alone may not reduce TB incidence. Comprehensive diagnostic strategies must address all phases of the disease, including subclinical TB, which remains difficult to diagnose. Developing reliable models is crucial to bridging the gaps in current procedures for diagnosing and treating this phase of TB [25].

The interaction between Mtb and macrophages is central to the progression of TB. These immune cells are the first to encounter Mtb during infection, attempting to engulf it through phagocytosis. However, Mtb has evolved mechanisms to evade destruction, including inhibiting phagosome maturation and preventing lysosome fusion. This allows Mtb to survive and replicate within macrophages, creating a protected intracellular environment.

Additionally, Mtb manipulates host immune responses by altering cytokine signaling and inhibiting apoptosis, supporting the formation of granulomas. Granulomas contain the infection but allow Mtb to persist in a latent state, complicating efforts to eliminate the disease by creating a reservoir of viable bacteria. Granulomas are composed of several resident cells (e.g., lung fibroblasts and epithelial cells), immune cells such as neutrophils, T-cells, and natural killer cells recruited by alveolar macrophages and by Mtb-infected alveolar macrophages [24].

After the infection is established, Mtb, like other bacteria, can go into dormancy.

In the dormant state, Mtb remains viable but inactive within infected cells or granulomas, avoiding immune detection and causing no symptoms. This dormant phase is key to the high proportion of individuals who remain asymptomatic and do not progress to active TB. Only about 5–10% of people infected with Mtb will develop active, symptomatic disease within the first five years, either shortly after infection or due to the reactivation of dormant bacteria later in life. When complete clearance does not occur, people develop what is called “latent infection”; this means that the host controls the pathogen's replication, and the individual remains asymptomatic but will be at risk of developing the disease in the active form during their lifetime [25,26].

Reactivation typically occurs when the immune system is compromised, such as in conditions like Human Immunodeficiency Virus (HIV) infection, malnutrition, or aging. This ability to switch between active and dormant states is central to the persistence and complexity of TB, making it challenging to diagnose and treat effectively [26].

Moreover, the Mtb capability to evade these host defenses by inhibiting phagolysosome formation, blocking phagosome acidification, expressing glycine-rich host proteins, and creating an electron-transparent zone (ETZ) that hinders the diffusion of lysosomal enzymes increases the Mtb to persist in the host.

Moreover, recent studies have confirmed that many external stress stimuli can lead to different molecular responses that result in transcriptional, posttranscriptional, or allosteric controls in Mtb [25].

Given the factors discussed earlier, it is easy to understand why drug-resistant Mtb strains are evolving. Mtb bacilli can become resistant to anti-TB drugs by acquiring genetic mutations and utilizing various mechanisms to adapt under selective environmental pressure. A significant contributing factor is heteroresistance, where subpopulations of Mtb within the same infection exhibit different levels of drug resistance, complicating treatment and eradication efforts [27].

The complex structure of granulomas poses additional challenges for drug penetration. The hypoxic and nutrient-deprived environment within granulomas can limit the efficacy of many anti-TB drugs, reducing their ability to reach therapeutic concentrations at the site of infection. These factors make treating drug-resistant TB particularly challenging, as genetic mutations and pharmacokinetic barriers contribute to the bacteria's survival and persistence [28].

How to study the pulmonary infection: *in vivo* models

As we said before, the organs comprising the respiratory system often serve as a first barrier against exogenous substances and act as a filter for the inhaled air, primarily at the microbial level. Consequently, many infectious diseases affect the entire respiratory system. For this reason, deepening our understanding of the physiological and pathological mechanisms operating within the respiratory tract has become essential. To do this, it has been necessary to develop models.

In vivo models identify models used in experiments conducted in living organisms. Animal models have been crucial in uncovering the biochemical and physiological mechanisms underlying cancer and infectious diseases for decades. They are still essential for evaluating the safety and efficacy of new drugs or implantable devices. However, these models inadequately replicate the histological structure of the human lung epithelium and demonstrate shortcomings in mimicking physical characteristics and physiological processes, such as cell-to-cell communication [4,29]. Moreover, the significant failure rates in clinical drug development and the challenges in translating preclinical animal data to human outcomes, alongside disparities between animal and human biology and human-specific pathogens, underscore the need for a paradigm shift towards advanced and validated human cell-based cultures [3].

Small animal models

Throughout history, small animal models, such as rodents and leporids, played a pivotal role as animal models for the study of pulmonary infections. Despite the limitations described above and better specified below, these models remain indispensable in preclinical TB research and have significantly contributed to the rapid progress in developing COVID-19 vaccines. Specifically,

mouse models are the most widespread and used animal models, even if they only partially recapitulate the complexity of human disease. On the contrary, other rodent species like rats, hamsters, and guinea pigs (Figure 3) offer valuable insights into pathophysiological aspects of respiratory infectious diseases that murine models may not fully capture.

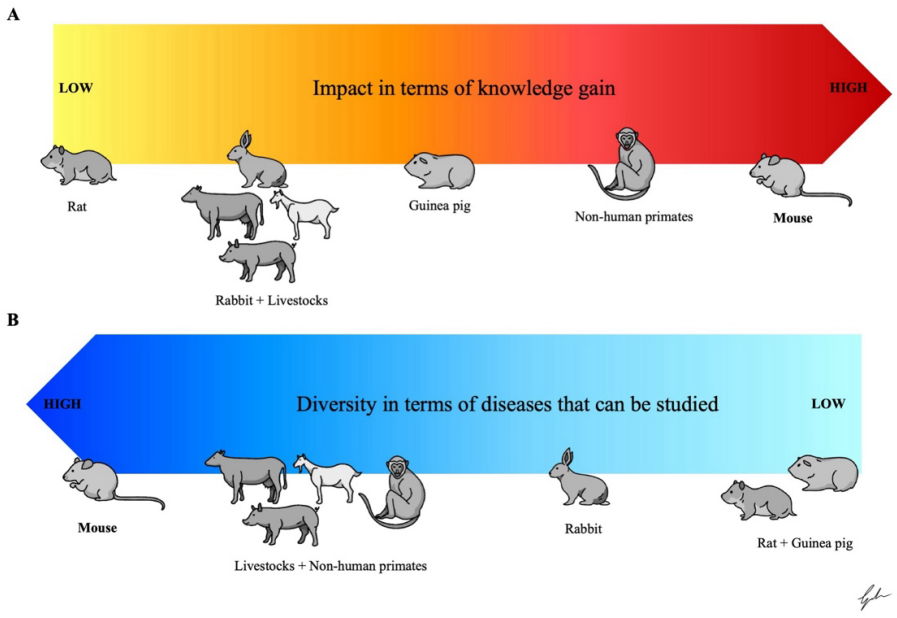

Figure 3. The figure represents a schematic overview of animal models for TB, reporting the diverse range of species used for studying these respiratory infections, from mice to non-human primates. Among these, murine models are the most varied, while guinea pigs, rabbits, hamsters, and livestock typically apply to only one of the two diseases. Non-human primates and mice have contributed the most to advancing knowledge, with non-human primates offering the highest translational value. Adapted from Corleis et al., "Animal models for COVID-19 and tuberculosis" Front. Immunol., 2023, published under the terms of the Creative Commons Attribution License (CC BY) [4].

Mouse model

Mice are the most used model for preclinical investigations due to their ease of handling, accessibility, affordability, and the extensive array of immunological and genetic tools available for research. Regarding Mtb infection, mice models are one of the first choices, considering their well-established nature in laboratory settings. However, while murine models offer numerous advantages, they also have limitations, particularly in fully capturing the complexities of TB infections [4,30].

The experimental murine TB model, achieved through aerosol exposure, has provided invaluable insights into the fate of the host following natural infection. It has meticulously delineated the intricate kinetics of the infectious process and facilitated the comprehensive integration of host and pathogen traits in experimental investigations.

However, mice do not fully replicate TB pathology observed in humans. Critical features such as granuloma liquefaction, cavitation, and fibrosis remain absent in Mtb-infected mice. Nonetheless, this model offers a platform to extensively examine immune responses to Mtb. The similarity between pulmonary anatomy and immune mechanisms in mice and humans makes mice well-suited to study immune dynamics within tissues and evaluate vaccine efficacy. Despite not being natural hosts for Mtb and generally exhibiting tolerance to the development of TB, mice have played a crucial role in elucidating specific disease mechanisms.

Overall, different aspects must be considered: host factors such as mouse genetics, age, sex, and immune status play pivotal roles in determining the outcome [31]. Additionally, variables including the route of infection, inoculum size, and bacterial characteristics such as Mtb lineages and virulence factors also significantly impact the progression of TB: exposure to different strains of Mtb in

mice results in distinct outcomes, with some strains triggering heightened susceptibility and granulomatous lesions resembling human pathology. Various genetic modifications in Mtb or host mice, such as deletion of virulence genes or immune-related genes, have been instrumental in elucidating the mechanisms underlying TB pathogenesis and host immune response.

Moreover, different strains of mice, including inbred, knock-out, collaborative cross (CC), and diversity outbred (DO) lines, have been employed to study TB. Inbred mice and knock-out lines have helped identify specific host factors essential for susceptibility to TB. In contrast, genetic diversity in CC and DO mice has facilitated the discovery of unbiased susceptibility or resistance traits [32].

In the end, it is essential to underline also the utility of transgenic mouse models in TB research. These models have provided insights into TB pathogenesis, including the role of immune cells, cytokines, and molecular pathways.

Rat model

Rats, particularly Wistar rats, are often involved in the pharmaceutical industry for pharmacokinetic and toxicological studies. They are also commonly present in immunization studies because of their widespread availability, ease of handling, well-defined physiology, and capacity to yield larger samples compared to mice.

Rats generally exhibit susceptibility to Mtb infection and have been utilized to discern investigational compounds' bacteriostatic or bactericidal properties [33]. Moreover, various rat strains, including American cotton rats, Lewis rats, Wistar rats, and Sprague-Dawley rats, develop granulomatous lesions that do not undergo liquefaction, thus failing to replicate human TB pathology

fully [34]. In the end, rats have also proven valuable in TB diagnostic endeavors, particularly in resource-constrained settings.

Guinea pig model

Guinea pigs are highly susceptible to TB: in his ground-breaking experiments, Robert Koch worked with guinea pigs and rabbits to demonstrate that pure cultures of Mtb cause the disease. They inhale mycobacteria and expel them through expectoration, akin to humans, making them suitable for transmission studies.

The course of TB infection in this type of animal varies based on the Mtb strain and initial dose, but invariably, animals succumb to Mtb infection. Following logarithmic lung growth, Mtb loads remain stable over many weeks. Toward the later stages of infection, Mtb bacteria can re-enter a logarithmic growth phase. Symptoms such as weight loss, labored breathing, and reduced activity are commonly observed, and this clinical observation aligns with histopathological findings of advanced disease. This later stage of infection is very similar to the humane endpoint. Granulomas in guinea pigs rarely exhibit liquefaction and cavitation [35], but they resemble primary lesions observed in humans more closely. Therefore, guinea pigs are not suitable for studying mycobacterial latency.

Guinea pigs are valuable for evaluating diagnostic skin tests and testing antimycobacterial compounds. Nonetheless, a drawback of the guinea pig model lies in the limited availability of immunological tools and genetically modified strains. Despite this limitation, recent advancements have seen the development of guinea pig-specific monoclonal antibodies and molecular screening techniques to study immune responses in greater detail [36].

Rabbit model

Rabbits are valuable models for studying the clinical features of Mtb infection [37]. The rabbit model closely reproduces post-primary TB, with animals developing cavities similar to human lesions involving bronchioles congestion, massive mycobacterial multiplication, and extensive necrotizing tissue destruction.

Moreover, also the outcome of Mtb exposure can be studied in rabbits, revealing that early innate inflammatory responses, inoculum size, and bacillary aggregation facilitate progressive TB and the development of pathology rather than the establishment of LTBI: TB pathology in rabbits, particularly the occurrence of cavities, mirrors the critical stage of the disease that is most relevant for successful antibiotic treatment.

The rabbit model is essential for studying the biodistribution of new and established antimycobacterial compounds. However, like guinea pigs, rabbits lack immunological reagents, which limits vaccinology studies. Additionally, the rabbit model is limited in replicating the clinical manifestations of TB. Furthermore, genetic editing of rabbits is still in its early stages, and the high costs compared to rodent models restrict the use of the rabbit model to specific scientific inquiries [38,39].

Large animal models

Livestock species and non-human primates (NHP) are natural hosts of the MTBC. Their similarity to humans regarding respiratory tract anatomy, lung structure (such as lobulation), and immune system organization and function makes them valuable models for studying respiratory diseases like TB and COVID-19. Their evolutionary proximity to humans provides additional advantages and unique insights into disease mechanisms.

Non-human primates model

Among NHP, Rhesus Macaques (RM), Cynomolgus Macaques (CM), and African Green Monkeys are commonly used for research on Mtb infection [40].

Depending on factors such as the dosage of Mtb administered (ranging from 101 to 105 colony-forming units), the specific Mtb strain utilized, and the method of infection (intravenous, intratracheal, or aerosol), RM and CM can accurately replicate the entire spectrum of TB seen in humans, including acute infection, LTBI, and reactivation of LTBI. Like humans, the granulomas observed in NHP exhibit mature, adaptive structures characterized by necrotic cores surrounded by layers of macrophages and lymphocyte zones, including areas of immunocompromised microenvironments. NHP granulomas also feature tertiary lymphoid structures, which are crucial in anti-mycobacterial immunity and mirroring human lesions.

Livestock model

Large livestock species, including cattle, goats, and pigs, are natural hosts and serve as models for human TB. While Mtb is a human-adapted strain, other members of the MTBC, such as M. orygis, M. caprae, and M. bovis, are zoonotic pathogens, with livestock species, including cattle, goats, and pigs, serving as their main reservoirs [41]. These bacteria can infect humans and cause pathology like Mtb-driven disease, often resulting in extra-pulmonary manifestations. Interestingly, while Mtb can infect livestock, such as cattle, it usually does not induce comparable pathology. Under experimental conditions, cattle, goats, and pigs can eradicate Mtb. Therefore, livestock species can serve as models for human TB to investigate pathologies, such as that induced by M. bovis, and correlates of protection against Mtb.

In all species, macrophages and their precursors, such as monocytes, serve as the main intracellular niche for M. bovis or Mtb [42].

Large livestock species offer unique opportunities to investigate disease susceptibility and resistance in natural hosts and are valuable models for novel preclinical vaccine concepts.

While experimentation with cattle may be challenging due to their size and associated costs, goats offer a viable alternative. Pigs provide additional advantages such as smaller size, lower costs, easier maintenance, and availability of immunological reagents. [43]. Further studies in large livestock species are warranted to elucidate their potential as models for human TB.

Limits and perspectives of the *in vivo* models

Using animal models in infectious disease research offers invaluable insights into host responses and disease pathogenesis under controlled conditions. However, it's essential to recognize that no ideal model exists for studying diseases such as tubercular infection (Table 1).

Table 1. Advantages and limits of the different *in vivo* models.

Model	Advantages	Limits	Applicability
Mouse	- detailed immunological insights - similarity to human anatomy and immune mechanisms - genetic diversity - feasibility of gene editing	- imperfect disease model (lack of granuloma liquefaction, cavitation, and fibrosis) - inadequacy for transmission studies	- immunological research: immune dynamics within tissues and vaccine efficacy - host susceptibility or resistance trait
Rat	- broad availability	- inadequate mirroring of	

	- easy handling - defined physiology - defined physiology - potential to obtain larger samples compared to mice	human TB pathology (the observed lesions do not fully replicate the liquefying lesions seen in human) - limitations in understanding TB pathophysiology	
Guinea Pig	- susceptibility to TB and transmission mode entirely similar to human - revealing disease mechanisms - human-like clinical presentation: guinea pigs develop granulomatous lesions similar to primary lesions in humans	- scarcity of immunological tools - lack of genetically modified strains - limited understanding of complex interactions	- vaccine efficacy - transmission studies - evaluation of diagnostic skin tests and antimycobacterial compounds
Rabbit	- rabbit model closely reproduces post-primary TB, including cavity formation	- lack of immunological reagents - limitations in clinical manifestation - infancy of genetic editing - high costs	- clinical features of TB: the post-primary phase - study of the antimycobacterial compounds
Non-human primate	- reflection of human TB spectrum (granuloma formation) - structural similarities	- high housing costs - ethical concern - shortage of animals - experimental variability	- monitoring disease progression: focusing on the role of tertiary lymphoid structures

			- co-infection studies
Livestock animals	- natural infection - granuloma formation - immune responses	- high housing costs and difficult logistic - ethical concern - experimental variability - translation to humans: risk	- transmission studies

Each animal model has benefits and limitations, and the purpose-oriented use of one or more models is essential for adequately addressing specific scientific questions and advancing interventions.

In conclusion, at the moment, targeted and well-considered use of animal models remains indispensable for understanding infectious diseases and testing vaccines or therapeutics. However, it must be pointed out that it is essential to follow the 3R concepts to reduce, replace, and refine the usage of animals in experimental research. These ethical-driven approaches represent the foundation of animal experimentation around the world, and it is conceivable that, in some cases, newer systems, such as three-dimensional cell culture or organoids, will continue to prove themselves to be able to replace some animal testing.

The 3Rs, "Replacement," "Reduction," and "Refinement"

The 3R principle—Replacement, Reduction, and Refinement—refers to a widely accepted ethical framework for animal research. Its main aim is to minimize the use of animals in research by replacing them where possible, reducing the number of animals used, and refining procedures to lessen their suffering. This ethical concept has firm roots. Introduced in 1959 by British scientists W. M. S. Russell and R. L. Burch, it is now incorporated into standard guidelines and regulations in many countries worldwide [44].

Even if the specific definition of the 3Rs might differ from one institution to another, it is generally accepted that “Replacement” deals with the possibility of alternative methods to minimize the use of animals as models in research [44,45]."Reduction" deals with the scientific question that analyses the experimental protocol to understand if it is possible to work with fewer animals than initially planned and explore whether parts of the problem can be investigated using non-animal testing methods. In the end, "Refinement" focuses on determining whether and how the suffering of laboratory animals can be minimized during an experiment or test.

Overall, as the directive 2010/63/EU specifies, the final goal of 3R is to completely replace animal research.

In “vitro” models

In vitro models are crucial in biomedical research. They offer a controlled environment for studying biological processes outside their natural context.

In vitro models are precious in studying Mtb infection because they allow exploring the interactions between the pathogen and the host immune system, which is not always achievable with *in vivo* models. This is particularly significant when considering the genetic variability of both the host (i.e., ethnic background) and the pathogen (different Mtb lineages). These factors can significantly influence infection dynamics and immune responses, making controlled in vitro systems indispensable for studying genetic and immunological intricacies.

In vitro systems allow researchers to investigate specific mechanisms and dynamic pathways that are challenging to study in animal models. Additionally, these models are indispensable for high-throughput drug screening, as they are more cost-effective and less resource-intensive than *in vivo* studies. They are

typically categorized into two-dimensional (2D) and three-dimensional (3D) cellular models, each providing unique insights into infection biology [18].

2D culture techniques have provided standardized and controlled conditions for experiments with living biological specimens. However, they have limitations due to the lack of a physiological microenvironment. The main limitations are (i) differences in substrate stiffness, (ii) absence of spatial cues, (iii) receptors topography, and (iv) differences in concentration gradients of nutrients and gases. It must be underlined that substrate stiffness and morphology significantly influence differentiation, migration, and gene expression.

3D models have emerged to overcome the limitations of 2D cultures. These models can potentially mimic physiological tissue behavior more accurately and at a lower cost than some animal models. By incorporating tissue complexity, 3D models provide a more physiologically relevant environment for studying various biological processes, including matrix remodeling, cell-cell interactions, growth factor secretion, and gene regulation [18].

The development of biological 3D multi-tissue models requires a multidisciplinary approach, integrating engineering, chemistry, physics, mathematics, biology, and physiology. These models offer promising avenues for studying human organ responses to external stimuli, cytofunctionality analysis, and the design of implant substrates.

Additionally, they reduce the need for small animal models, aligning with the principles of the 3Rs (reduce, replace, refine) in animal experimentation.

In summary, 3D in vitro models represent a pivotal tool for evaluating essential biological processes in a physiological context, providing valuable insights into cell interactions and reducing the reliance on animal models in research.

Cell culture of human airway epithelial cells: focus on 3D models and their application in the study of the tubercular infection

Nasal, tracheal, bronchial, small airway, and alveolar epithelial cells can be cultured using various techniques, including submerged conditions, air-liquid interface (ALI) culture, lung-on-a-chip systems, or in organoid form (Figure 4) [46].

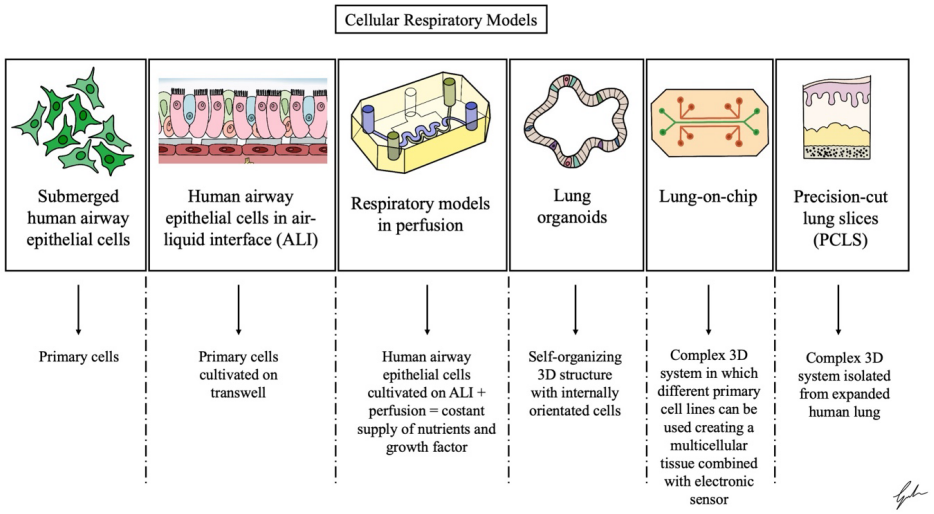

Figure 4. Schematic summarization of the most common 3D model used for reproducing the human airways. Adapted from Dichtl et al., "The breathtaking world of human respiratory in vitro models: Investigating lung diseases and infections in 3D models, organoids, and lung-on-chip" Eur.J.Immuno, 2024, published under the terms of the Creative Commons Attribution License (CC BY) [18].

These cell culture models aim to mimic the characteristics of epithelial cells from their specific region within the human respiratory tract or lung *in vivo*. These models represent different types of epithelial cells, mirroring the diversity observed in the human lung. These include club, ciliated, basal, and goblet cells.

Submerged and ALI culture

Human airway epithelial (HAE) cells derived from primary tissue offer a promising opportunity to study the human lung epithelium in various experimental setups. When HAE cells are cultured in a submerged environment, they are typically grown on plastic surfaces coated with extracellular matrix proteins like collagen or cellulose. This method yields primarily basal cells distributed throughout the airway tree but results in the loss of differentiated ciliated and secretory cells.

The air-liquid interface (ALI) culture technique has been developed to address these shortcomings and create a more physiologically relevant model. In ALI culture, HAE cells are seeded onto microporous membranes coated with matrix proteins, exposing the apical side of the cell layer to air. In contrast, the basolateral side remains submerged in a nutrient medium. This setting enables HAE cells to undergo differentiation into a pseudostratified mucociliary epithelium, encompassing various functional cell types, including basal, ciliated, and mucus-secreting goblet cells.

ALI-cultured HAE cells offer a closer representation of the *in vivo* lung environment. Additionally, ALI culture presents the advantage of exposing the cells to pathogens or airborne substances, facilitating studies on host-pathogen interactions and respiratory toxicology [47].

Organoids

Organoids represent 3D structures autonomously forming tissue architectures resembling airways [48]. They mirror the critical characteristics of their respective organs. These respiratory cell aggregates originate from stem or progenitor cells sourced from adult or embryonic tissues or induced pluripotent stem cells (iPSCs) [49].

Typically, organoids derived from adult stem cells (ASCs) exhibit polarized, cystic structures primarily composed of epithelial cells. These structures are less complex than organoids derived from pluripotent stem cells (PSCs), which also contain non-epithelial cell types. The choice of stem cell source significantly influences the cellular composition of lung organoids. Human PSC-derived organoids tend to display an alveolar phenotype, predominantly containing alveolar type I (AT1) and type II (AT2) cells.

Conversely, organoids obtained from adult tissue biopsies or bronchoalveolar lavage fluid present a broader range of cell types, including basal, club, goblet, and ciliated cells [50].

While lung organoids contain fewer basal cells than HAE cells, they feature a higher abundance of club and ciliated cells.

Organoids are typically embedded in a matrix like Matrigel or cultured in 3D systems like the Celvivo system. These organoids maintain an internally oriented ciliated apical surface, which poses experimental challenges. Consequently, methods have been devised to reverse the epithelial polarity and expose the apical surface outward. Strategies to enhance proximal differentiation include inducing ciliary differentiation in alveolar organoids, which results in an increased presence of ciliated, basal, and goblet cells while decreasing club cell populations.

Human organoid cultures can be differentiated on transwell inserts or as monolayers in submerged cultures [51].

Monolayer cultivation predominantly yields a distal signature with AT1 cells, suggesting a bias towards AT2 differentiation into AT1 cells. In contrast, ALI-cultured lung organoids comprise ciliated, goblet, and basal cells, forming a proximal pseudostratified mucociliary epithelium.

Lung on chip

The "lung-on-chip" model utilizes complex 3D systems comprising primary cells, cell lines, PSCs, or ASCs on engineered microdevices. This model mimics the *in vivo* environment by incorporating multicellular tissues, which can be integrated with electronic sensors for real-time organ and tissue function monitoring.

Additional advantages include the combination of engineered microtissues with microfluidic devices, enabling the application of mechanical forces such as stretch and shear, fluid flow, biochemical cues, and electrical or optical signals [52,53].

Co-culture with immune components

HAE or lung organoids cultured on a transwell—submerged or in ALI—can be supplemented with other cells, such as immune cells.

The respiratory immune system is increasingly recognized for maintaining epithelial barrier integrity and lung homeostasis. Even epithelial disruption triggers massive production of innate immune components, leading to inflammation or immune cell recruitment. Nonimmune epithelial cells can release innate immune responses like intracellular complement and cytokines. Therefore, incorporating immune cells or characterizing humoral immune components at infection sites is crucial for bridging the gap between in vitro models and the host situation.

During initial pathogen invasion, dendritic cells (DCs), macrophages, natural killer cells, and neutrophils synergistically promote airway inflammation, cytokine release, and lysis of infected cells.

DCs, as immune sentinels, process antigens and transition from immature to mature cells, initiating adaptive immunity. Including these known modulators

of respiratory barrier functions in in vitro models is essential for better mimicking the host environment. Immune cells are typically added on the basolateral side, interacting with epithelial cells through cell-cell contact or cytokine release.

Co-culture models, such as neutrophils with HAE cells, macrophages with HAE or SAE cells, or dendritic cells with HAE cells, are essential, especially for studying infection at entry sites [18,47].

Co-culture of airway epithelium with peripheral blood mononuclear cells allows the analysis of innate and adaptive immune subsets during infection over time. Incorporating immune cells like NK or CD8 T cells requires matching the HLA phenotype between immune and epithelial cells [49,54,56].

Respiratory models in perfusion and Precision-cut lung slices

Microphysiological systems, like organs-on-chip and interconnected 3D tissue constructs, provide more relevant alternatives to traditional cultures or animal studies, especially for studying human pathogen interactions at barrier sites. In vitro microfluidic models for the respiratory tract, including the alveolar level, mimic respiration and vascularization, offering a more accurate representation. These systems continuously evolve to incorporate the respiratory microenvironment's physical, mechanical, and organizational features [57].

Perfused conditions in microfluidic models significantly enhance ciliogenesis and mucus production compared to static cultures. This is attributed to the increased nutrient supply and enhanced cell communication.

Precision-cut lung slices from human lungs offer another ex vivo model maintaining microarchitecture and function, enabling mechanistic studies.
However, their viability is typically limited to 7-10 days, with changes in tissue architecture over time posing some limitations. Despite this, precision-cut lung

slices remain valuable for controlled lung physiology and pathology investigations.

In Vitro Granuloma Models of Tuberculosis

Despite extensive research, many fundamental aspects of TB pathogenesis remain elusive. The intricate interplay between the host and the pathogen, particularly within multicellular tissue granulomas, is a crucial challenge.

Granulomas are complex structures composed of various cell types. They are predominantly mature macrophages at the core surrounded by T cells, B cells, and fibroblasts. They are formed in response to persistent stimuli (Figure 5).

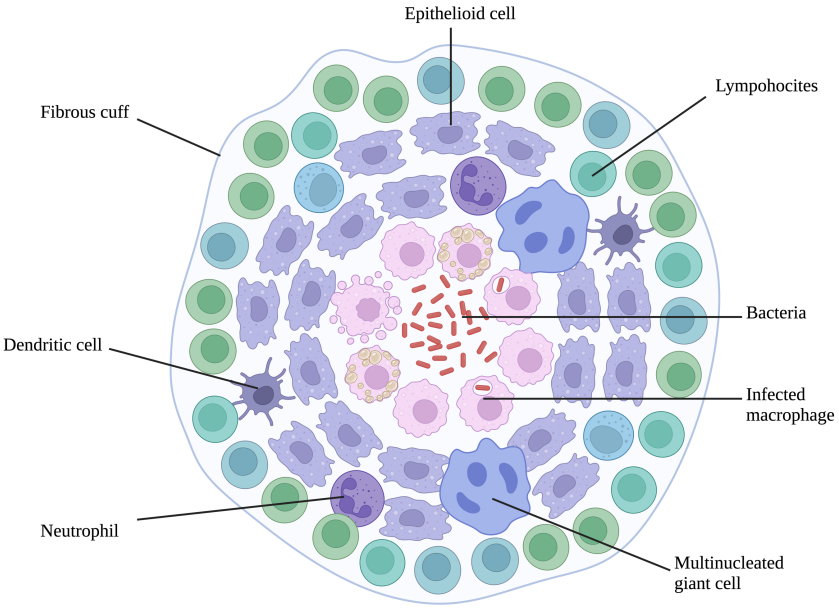

Figure 5. Schematic representation of the main cellular component of a granuloma. Created in BioRender. https://BioRender.com/m59m113.

While granulomas have been observed for centuries, the mechanisms governing their dynamics, behavior, and maintenance are now being elucidated [58].

Contrary to traditional views, in which granulomas have always been represented as a way of limiting infection, recent findings from the zebrafish model suggest that in Mtb infection, they may promote mycobacterial growth and spread.

For this reason, understanding the molecular basis of macrophage reprogramming and specific cellular events within TB granulomas, like multinucleate giant cell formation and central necrotic caseation, still needs to be completed.

Cell culture systems of TB granulomas

Collagen Matrix Model of Mtb Dormancy

Kapoor and colleagues [53] developed a 3D model that employs human peripheral blood mononuclear cells (PBMCs) within an extracellular matrix to recreate spatially and temporally accurate three-dimensional structures and microscopic granulomatous aggregates in response to virulent Mtb. This model effectively mimics key features of human TB, such as multinucleated giant cell formation, changes in T cell populations, macrophage activation status, and increased cytokine and chemokine secretion upon Mtb exposure.

A crucial aspect of this model is its ability to simulate Mtb latency and reactivation under immune suppression induced by anti-tumor necrosis factor-alpha (anti-TNF-α) treatment. Thus, it offers insights into host-pathogen interactions during latency and reactivation. It also showcases fundamental latency characteristics, including non-replicating states, rifampicin resistance, loss of acid fastness, and lipid body accumulation.

Despite its strengths, the model has limitations such as low throughput, technical challenges in adding cells over time, and the need for collagenase to release cells from the matrix for analysis. Nonetheless, its potential to advance

our understanding of Mtb latency and reactivation and identify therapeutic interventions remains promising [59].

Multicellular Lung Tissue Model

Lerm and colleagues introduced Mtb into a human in vitro lung tissue model to investigate early granuloma formation [60]. This model involves a collagen matrix supported by a filter membrane acting as a scaffold for a human fibroblast cell line, which grows and differentiates before the addition of primary macrophages/monocytes and a human epithelial cell line.

Once tissue formation occurs, the apical side is exposed to air, stimulating mucus secretion by the epithelial cells. This organotypic mucosa closely resembles lung tissue both anatomically and functionally.

Studies in zebrafish and human lung tissue models suggest that Mtb virulence factors are involved in the induction of granuloma formation. For instance, host matrix metalloproteinases (MMPs) induced by mycobacterial virulence factors are known to promote granuloma formation [61]. Inhibition of MMPs has been shown to reduce both granuloma pathology and bacterial load in the human lung tissue model, aligning with reports advocating for MMPs inhibition in mouse models of TB.

This model's limitations include (i) challenges in introducing other immune cells, such as lymphocytes or neutrophils, and (ii) adapting it for high-throughput assays. Nevertheless, the model can potentially study host-pathogen interaction and secondary assays for assessing novel TB drugs.

Granuloma Model to Assess the Impact of the Human Immune Response

Guirado et al., developed a granuloma model using human PBMCs and autologous serum to mimic the immune environment typical of Mtb infection [8]. Indeed, this innovative system allows the study of early granuloma formation.

The model was developed to study the immunopathogenesis of individuals with LTBI. The authors demonstrated that LTBI subjects exhibit significant differences in bacterial survival, immune cell activity, cytokine production, and lipid body accumulation, highlighting variations in immune responses and their effects on granuloma formation. Additionally, it highlights a unique bacterial transcriptional signature influenced by the host's immune status. The model's ability to simulate these interactions demonstrates its potential for personalized medicine and advances in TB biomarker and treatment research.

Limitations of the initial model, such as the absence of fibroblasts and extracellular matrix components, have been addressed, influencing the kinetics and stability of granuloma formation. Additionally, the model lacked a continuous influx of mononuclear phagocytes needed for sustained dynamic structures, leading to the introduction of HIV into the model to explore its impact on granuloma formation and dissolution timing.

This model allows comparative analysis with other granulomatous diseases and can be adapted for high-throughput screening of potential therapeutic compounds. Continuous refinement and development of this system offer promise for advancing the understanding of granuloma biology, exploring therapeutic interventions, and studying the effects of comorbidities.

Bioelectrospray 3D Model

Workman et al., developed an innovative system based on cell encapsulation within microspheres, achieved through alginate cross-linking in a calcium chloride bath [62]. This technique produces highly customizable microspheres with a matrix and cellular composition conducive to manageable experimentation. Cells can be quickly released from the spheres for downstream analysis by dissolving them in solutions like EDTA or sodium citrate.

This system has been utilized to explore various aspects of the host-pathogen interaction and has several translational applications. Initially, comparisons between spheres with or without collagen revealed the regulatory role of the extracellular matrix in the host-pathogen interaction, consistent with findings from transgenic mouse studies. Subsequently, the group investigated different dimensions of the host immune response, including studies on spheres exposed to various cytokines or featuring enhanced Mtb-responsive T cells [63].

Integrating diverse cell types into multiple spheres and examining their effects over extended periods (up to 21 days) offers an effective tool for discerning protective versus pathological immune responses. Notably, Mtb exhibits sensitivity to pyrazinamide when cultured in three-dimensional microspheres, replicating stress conditions encountered *in vivo*. Moreover, due to the confinement of cells and bacteria within the microspheres, the model lends itself to microfluidic pharmacokinetic modeling. In this setup, increasing concentrations of rifampicin have been demonstrated to accelerate Mtb killing.

Additionally, the model has been used to explore the effects of MMPs inhibition with doxycycline in limiting TB-driven immunopathology.

This model faces challenges like other systems, including difficulties incorporating additional immune cells after encapsulation within the microspheres. Further refinements address these limitations by introducing a dual encapsulation system to mimic better granuloma features, such as a caseous central core and an oxygen gradient from the periphery to a hypoxic center (cause). These advancements could also facilitate cellular intake, enabling the model to simulate immune cell recruitment to granulomas more effectively, thereby enhancing its utility for studying TB immunopathogenesis.

Lessons From Animal Models

The complexity of chronic host-pathogen interactions in human TB necessitates using animal models alongside in vitro systems. While in vitro models with human cells offer valuable insights, they lack the full complexity observed in human disease.

Conversely, animal models provide a more comprehensive understanding of these interactions, and their findings inform the development of human systems.

Classically described granulomas in TB have a characteristic architecture, typically consisting of a caseous center surrounded by layers of myeloid and lymphocytic cells. These lesions may eventually become necrotic or fibrotic, leading to mineralization or cavitation. Signaling cascades involving myeloid cells and interferon-gamma from T cells aim to eliminate Mtb within the lesion. Still, sterilization is rarely achieved due to the complex granuloma environment, which promotes and inhibits bacterial killing. As we saw before, traditional mouse models do not fully replicate the specialized architecture of human lung TB granulomas. However, recent developments have allowed for generating necrotic or fibrotic lesions in mice. Other animal models, such as guinea pigs, rabbits, and macaques, develop granulomas more akin to those observed in humans, including necrotic and organized structures, with hypoxia particularly prominent in necrotic regions. Under specific conditions, rabbits have been used to study cavitary lesions, further highlighting the relevance of animal models in understanding TB pathogenesis.

These animal models provide crucial insights into the mechanisms within lung granulomas that drive the balance of Mtb killing and survival.

Conversely, 3D models are particularly useful in studying Mtb because they closely replicate granulomas' structural and functional complexity, which is

central to TB pathology. These models provide a controlled environment that allows researchers to investigate the interaction between Mtb and host immune cells.

Crucially, 3D models enable the assessment of the genetic background of both the host (e.g., ethnic variability) and the pathogen (e.g., Mtb lineages). This is important as both factors significantly influence infection outcomes and immune responses. Unlike traditional 2D or animal models, 3D systems can integrate human-relevant genetic and immunological diversity, facilitating more precise studies on how these variables shape granuloma formation, pathogen persistence, and immune evasion mechanisms.

Additionally, 3D systems can mimic oxygen gradients, nutrient limitations, and the architecture of granulomas more effectively than other models, making them indispensable tools for drug testing and personalized medicine research.

Chapter 2: From Antioxidants to Inflammation: The Role of Oxidative Stress in Pulmonary Health and Disease

The lung, with its extensive surface area and rich blood supply, is uniquely exposed to atmospheric oxygen, making it highly susceptible to oxidative injury [64]. This vulnerability arises from the lung's continuous interaction with reactive oxygen, nitrogen species (ROS/RNS), and free radicals generated endogenously and exogenously [65].

Oxidative stress plays a critical role in the pathogenesis of various lung diseases, including chronic obstructive pulmonary disease (COPD), asthma, pulmonary fibrosis, and acute lung injury. Oxidative stress refers to an imbalance between ROS, RNS, and antioxidants that leads to damage to cellular components like lipids, DNA, carbohydrates, and proteins. Moreover, beyond localized damage, these oxidized biomolecules can trigger systemic cellular responses by generating secondary reactive metabolites, further amplifying oxidative damage and contributing to broader pathological processes [66].

In the lung, ROS/RNS are primarily generated by phagocytes and various lung cells, including polymorphonuclear, alveolar, bronchial, and endothelial cells. In addition, oxidative stress is critical in the pathogenesis of diffuse lung diseases, such as idiopathic pulmonary fibrosis, by promoting inflammation, fibrosis, and tissue damage, exacerbating the disease progression. Moreover, ROS can activate different signaling pathways that release pro-inflammatory cytokines, chemokines, and growth factors, worsening the disease's progression and the patient's clinical presentation, particularly in conditions like asthma and COPD. In these cases, in fact, prolonged oxidative stress can lead to structural changes in the lung, such as airway smooth muscle hyperplasia, fibrosis, and mucus hypersecretion. These changes result in airway narrowing and impaired

lung function. Moreover, oxidative stress affects the endothelial cells of the lung's blood vessels, leading to increased vascular permeability and edema, commonly observed in acute lung injury and in acute respiratory distress syndrome. In the end, ROS-induced damage to alveolar epithelial cells can cause cell death and impair the integrity of the alveolar-capillary barrier [65].

Oxidative sources in the lung

The accumulation of inflammatory cells like macrophages and neutrophils in the lower respiratory tract can lead to an increased oxygen burden in the lungs, triggering excessive production of ROS. Among them, many are the free radicals that could be produced. Among them, the most notable with physiological significance are superoxide anion ($O_2\bullet^-$), hydroxyl radical (•OH), nitric oxide (NO), and hydrogen peroxide (H_2O_2) [67,68].

ROS plays a crucial role in fibrogenesis and oxidative stress, influencing cytokines and growth factors involved in inflammation and lung fibrosis. For example, oxidative damage is evident in idiopathic pulmonary fibrosis and other lung disorders. Moreover, ROS also contributes to smoking-related COPD and carcinogenesis.

The mitochondria in non-phagocytic cells are the primary source of ROS, although other cellular structures, such as the smooth endoplasmic reticulum and microsomes, also contribute. Under normal conditions, ROS are involved in critical physiological processes, such as apoptosis, gene expression regulation, and immune defense. However, when it leads to oxidative modification of proteins, notably through carbonylation, it becomes a hallmark of oxidative stress and a biomarker for protein damage in pulmonary diseases. [69]

In addition to endogenous generation, exogenous exposition plays a crucial role in defining oxidative stress production in the lung (Figure 6).

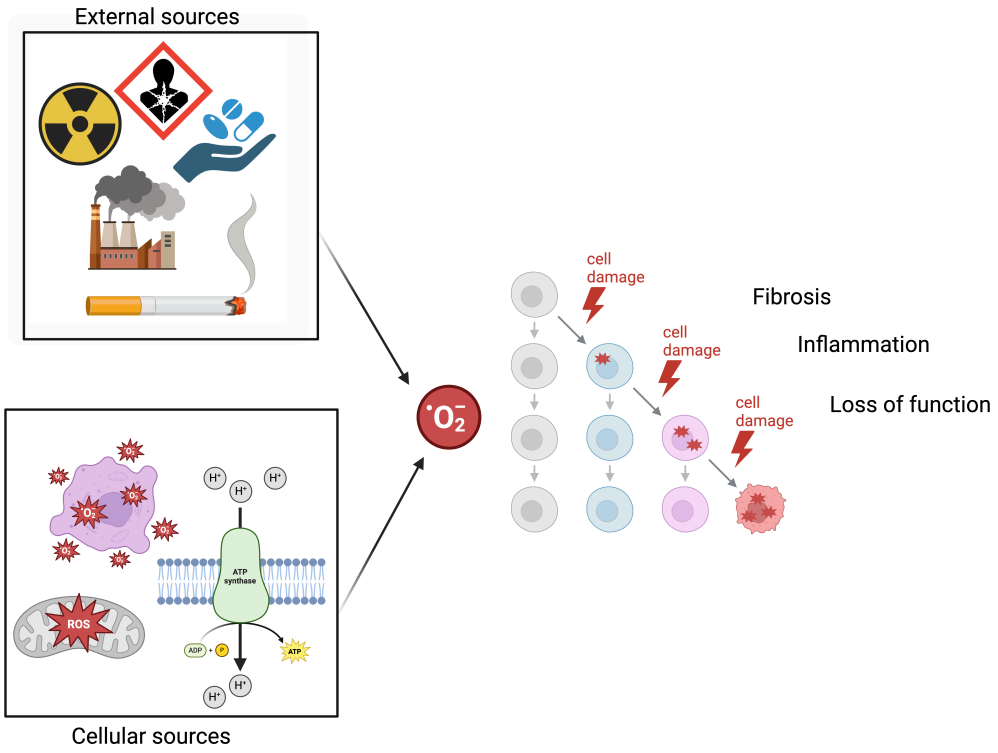

Figure 6. Schematic representation of the main pathways involved in the cascade activated in the lung after the exposition to endogenous and exogenous oxidative stimuli. Created in BioRender. https://BioRender.com/m59m113.

CS and airborne pollutants, such as ozone, nitrogen dioxide, and particulate matter, damage the lungs and heightened inflammatory responses.

In particular, CS is a complex mix of over 4,700 chemical compounds across its gas, aqueous, and tar phases. The gas phase contains high levels of oxidants and free radicals, O2•− and nitric oxide, which combine to form the reactive peroxynitrite molecule. The tar phase houses organic radicals like semiquinone, capable of redox cycling with biological reducing agents (e.g., ascorbate, NAD(P)H, and glutathione), perpetuating the production of superoxide radicals. This process can continue in the epithelial lining fluid of

smokers. The tar phase also chelates metals like iron, generating hydrogen peroxide.

Sidestream CS is particularly harmful, containing over 10^{17} reactive organic compounds per puff, such as carbon monoxide, formaldehyde, and carcinogens like benzo(a)pyrene. These compounds, concentrated in the lung's epithelial lining fluid, significantly contribute to oxidative stress and respiratory damage.

The molecular pathways associated to the oxidative stress imbalance

Oxidative stress plays a significant role in the regulation of extracellular matrix (ECM) degradation, a key process in the pathogenesis of diffuse lung diseases (DLD) like idiopathic pulmonary fibrosis (IPF). Structural remodeling is driven by matrix metalloproteinases (MMPs) and their inhibitors, tissue inhibitors of metalloproteinases (TIMPs). Increased expression of MMPs, particularly MMP-7 (matrilysin), has been observed in the lungs of IPF patients, contributing to epithelial damage. ROS/RNS exacerbate protease/antiprotease imbalances by activating MMPs, modifying their cysteine domains, and inactivating TIMPs [70,71].

ROS/RNS can intervene in the balance of the apoptotic process by interacting with key mediators of this pathway, such as the caspases. Apoptosis plays a crucial role in lung homeostasis and in the pathogenesis of fibrotic lung diseases. The caspase cascade is activated through intrinsic or extrinsic pathways, leading to cell death: ROS/RNS contribute to apoptosis by activating caspases, inducing cytochrome C release from mitochondria, and triggering DNA fragmentation. ROS/RNS also interact with the MAPK pathway, activating ERK, JNK, and p38 MAPK, further promoting cell death.

TGF-β is another important profibrotic cytokine. It is overexpressed in IPF lung tissue, promoting fibroblast activation, ECM production, and abnormal lung tissue remodeling. ROS/RNS regulate TGF-β activity by activating NADPH oxidase, which increases ROS production and enhances the activation of latent TGF-β. ROS also impairs glutathione synthesis, contributing to the antioxidant deficit characteristic of IPF [72].

The antioxidant activity of the lung

The body relies on antioxidants as a primary defense against oxidative stress, with two main categories of antioxidants: non-enzymatic (e.g., vitamins E and C, β-carotene, glutathione) and enzymatic antioxidants (e.g., enzymes in the glutathione redox system such as glutamate cysteine ligase, glutathione reductase, glutathione peroxidase, glucose-6-phosphate dehydrogenase, superoxide dismutases, catalase, heme oxygenase-1, peroxiredoxins, thioredoxins, and glutaredoxins). These antioxidants often work together, recycling each other to maintain a balance in the cellular redox state.

The primary enzymatic antioxidants in the lungs are SOD, CAT, and glutathione peroxidase. Recently, heme oxygenase-1, small molecular weight redox proteins such as thioredoxins, peroxiredoxins, and glutaredoxins, have also been found to play a crucial role in lung antioxidant defense mechanisms [73].

SOD is mainly known because it is present in almost every cell in the body and plays an essential role in protecting cells and tissues against oxidative stress. Three forms of SODs are classified based on their structure, localization, inducibility, and metal ion requirements.

Next, CAT is known for being a homotetrameric protein (MWt 240 kDa) that decomposes hydrogen peroxide into water and oxygen. It is found in most

aerobic cells in animals, especially in the liver and erythrocytes, but it is present in low amounts in the brain, heart, and skeletal muscle. It is concentrated in peroxisomes and the cytoplasm, and it is localized in alveolar type II pneumocytes and macrophages [70]. CAT is the most critical antioxidant enzyme in consuming exogenous hydrogen peroxide in rat type II pneumocytes. Moreover, CAT is the only antioxidant enzyme whose levels increase at the mRNA and activity levels during human lung morphogenesis [74].

Heme oxygenase (previously known as heat shock protein 32) is a member of the heat-shock family of proteins that plays a protective role in inflammation and oxidative stress [75]. It catalyzes the degradation of heme into bile pigments (biliverdin) in a reaction that generates carbon monoxide and iron [76]. Many stimuli, such as hyperoxia, hypoxia, lipopolysaccharide, and oxidative stress, induce heme oxygenase. It has been shown to have cytoprotective capacities. Also in this case, three isoforms of heme oxygenase (heme oxygenase-1, -2, and -3) have been characterized, where heme oxygenase-1 is inducible, while heme oxygenase-2 and -3 are constitutive [77,78].

In the end, the GSSG/2GSH ratio is a good indicator of the cellular redox state [79]. This ratio in GSH parlance can be determined by the rates of hydrogen peroxide reduction by glutathione peroxidase and GSSG reduction by glutathione reductase. The intracellular redox status of lung epithelial cells is critical in determining cell susceptibility or tolerance to oxidative insults. Studies have shown that GSH depletion, due to glutamate cysteine ligase inhibition by butathionine sulfoximine, sensitizes A549 cells, for example, to the injurious effects of hyperoxia and hydrogen peroxide, resulting in increased membrane permeability and activation of NF-κB [65].

The role of oxidative stress in the Mtb lung infection

Respiratory tract infections caused by bacterial pathogens result from a combination of increased bacterial adhesion, compromised immune defenses, and predisposing conditions such as COPD and asthma. The airway epithelium is a primary defense mechanism, serving both as a physical barrier and an active participant in immune responses. Through pattern recognition receptors (PRRs), epithelial cells detect bacterial pathogens and activate pro-inflammatory pathways that limit pathogen proliferation. Specifically, epithelial cells in the bronchi and alveoli recognize Mtb using Toll-like receptors (TLRs) and NOD-like receptors (NLRs), as described by Leiva-Juarez et al. [80,81].

However, bacterial infections often lead to excessive production of reactive oxygen species (ROS) during immune responses, resulting in oxidative stress that damages tissue, impairs epithelial function, and disrupts immune regulation. This mechanism is particularly evident in the early stages of Mtb infection, where oxidative stress plays a significant role.

External factors such as nicotine—a major component of CS—exacerbate oxidative stress and further compromise immune defenses. Nicotine inhibits the production of antimicrobial peptides, such as LL-37 and β-defensins, in lung epithelial cells, reducing their ability to control Mtb growth. Additionally, nicotine disrupts macrophage functions, including phagosome-lysosome fusion and autophagy, which are critical for the clearance of intracellular bacteria. These effects are mediated by the activation of nicotinic acetylcholine receptors (nAChRs), which alter immune signaling and promote the release of immunosuppressive cytokines, such as transforming growth factor-beta (TGF-β), by regulatory T cells (Tregs) [82].

The combined effects of nicotine and oxidative stress amplify lung damage and create an environment conducive to Mtb persistence and disease

progression. The interplay between oxidative stress and immune suppression highlights the impact of nicotine on TB pathogenesis. Epidemiological evidence linking smoking prevalence to increased TB incidence underscores the need to prioritize smoking cessation as a key strategy in TB prevention. Addressing both microbial control and the reduction of oxidative stress is essential for effective TB management, particularly in populations with high smoking rates.

Chapter 3: Aim of the thesis

This thesis aims to investigate the impact of nicotine-induced oxidative stress on the cellular components of the pulmonary microenvironment, with a particular emphasis on lung epithelial cells and their susceptibility to *Mycobacterium tuberculosis* (Mtb) infection. Given the complex interplay between the host immune response and Mtb in tuberculosis (TB) pathogenesis and the challenges of developing reliable *in vivo* models, this research employs an advanced three-dimensional (3D) printed lung model. This model, integrating lung fibroblasts (LF-hTERT), bronchial epithelial cells (HBEC-3kt), and monocytes (THP-1), provides a more accurate representation of the pulmonary microenvironment compared to traditional two-dimensional (2D) cultures. The 3D model, by closely mimicking the structural and functional characteristics of lung tissue, allowed for a detailed exploration of external stimuli effects, possibly offering new insights into the mechanisms by which molecules, such as nicotine, modulates host-pathogen interactions.

Additionally, this study aims to highlight the critical role of oxidative stress in compromising epithelial barrier integrity, mainly through the disruption of tight junctions. This research underscores the need for further investigations into the oxidation and degradation of tight junction proteins and the broader oxidative damage in the lung microenvironment caused by nicotine and Mtb.

By establishing a cause-and-effect relationship between nicotine exposure and TB infection dynamics, this thesis aims to inform the development of targeted strategies to mitigate smoking-related TB progression, with the ultimate goal of reducing infection rates and improving disease prevention efforts.

Chapter 4: Materials and Methods

Plasmid Description

The reference strain H37Rv was engineered with an integrative plasmid carrying a constitutively expressed fluorescence protein to allow the tracking of Mtb during infection.

The mycobacterial plasmid was designed to include the phage attachment site (attP) from the mycobacteriophage L5 genome and the bacterial attachment site (attB), enabling integration into the mycobacterial chromosome. Integration occurs via recombination between the plasmid-borne attP site and the chromosomal attB site, mediated by the L5 integrase (int) gene carried by a mycobacterial vector.

This plasmid also features an origin of replication (ori), a polylinker region containing restriction sites recognized by enzymes (BamHI, EcoRV, ScaI), and a hygromycin resistance cassette (Hyg) for selection in mycobacteria. These components enable the construction of mycobacterial strains expressing mCHERRY to track bacterial infections using confocal microscopy. mCHERRY exhibits an absorption spectrum of 540–590 nm and an emission range of 550–650 nm.

Electroporation

Electroporation was conducted using the Bio-Rad apparatus (Ec2-Bacteria, 2500 V, 25 μF, and 200 Ω), 50 μL of competent H37Rv cells was mixed with 2μg of plasmid DNA and incubated on ice for 1 minute. The mixture was then transferred to an electroporation cuvette and pulsed. Post-electroporation, 1 ml of liquid medium was immediately added to the cells, and the culture was incubated at 37°C with 5% CO_2 for 24 hours to allow recovery and plasmid expression before plating on selective agar (7H10+10% OADC+ Hygromycin 100

μg/mL), so that at 37 ° C for about four weeks. A mutant subclone was selected, expanded in 7H9 enriched with 10% OADC, 0.05 Tween 80, and Hyg 100 μg/mL, and incubated at 37 °C. A PCR was performed on DNA extracted from the mutant H37Rv (H37Rv_mCHERRY) to confirm the plasmid integration.

HBEC3-KT bronchial epithelial cells

HBEC3-KT (Evercyte, Leberstrasse 20, 1110 Vienna, Austria) is a human bronchial epithelial cell line derived from cells of a central lung bronchiole immortalized by transfection with a retroviral construct containing human telomerase (hTERT) and mouse cyclin-dependent kinase 4 (CDK4).

This cell line retains the expression of the epithelial stem/progenitor cell marker tumor protein p63 (p63). Moreover, it can differentiate into ciliated and goblet cells if seeded on a contracted fibroblast matrix and raised to an air-liquid interface for four weeks.

The HBEC3-KT are cultured in Keratinocyte-SFM supplemented with Bovine Pituitary Extract and Epidermal growth factor (compKSFM) at 37 °C in a humidified atmosphere with 5% CO_2. When at 80% confluence, the cells are passed using trypsin-EDTA (Euroclone, Milan, Italy) to ensure appropriate cell culture conditions.

For infection experiments, $2{,}5\times10^4$ HBEC3-KT cells were plated in a Tissue culture treated 24-well plate.

Infection was carried out using H37Rv_mCHERRY at an exponential growth phase (OD_{600}: 0.4–0.6) with a multiplicity of infection (MOI) of 100:1. After infection, cells were washed, lysed with sterile water at 37°C for 30', and serially diluted 1:10 to be seeded for the CFU count. Alternatively, cells were incubated with a 10% AlamarBlue solution for 2 hours for the viability assays.

hTERT Lung Fibroblast

hTERT-HLF (Evercyte, Leberstrasse 20, 1110 Vienna, Austria) is a human hTERT-immortalized lung fibroblast cell isolated from a female patient's lung and immortalized via transfection with the catalytic subunit of the human telomerase (hTERT) gene.

This cell line retains the expression of TGF-Beta-induced Alpha-smooth muscle actin. Moreover, the toxicity induced in hTERT-HLF after exposure to chlorhexidine (CHX) is similar to that induced in primary lung fibroblasts, suggesting that hTERT-HLF can be an excellent model for investigating toxicity.

The hTERT-HLF are cultured in DMEM/F12 (1:1, Sigma-Aldrich, St. Louis, Missouri, USA), enriched with stable Glutamine, 10 % FBS (Euroclone, Milan, Italy) and 200 μg/ml G418 (Sigma-Aldrich, St. Louis, Missouri, USA) and were maintained at 37 °C in a humidified atmosphere with 5% CO_2. The cells were passed using Acutase (Sigma-Aldrich, St. Louis, Missouri, USA) when at 80% of confluence to ensure appropriate cell culture conditions.

For infection experiments, $2{,}5\times10^4$ hTERT-HLF cells were plated in a Tissue culture treated 24-well plate.

Infection was carried out using H37Rv_mCHERRY at an exponential growth phase (OD_{600}: 0.4–0.6) with a multiplicity of infection (MOI) of 100:1. After infection, cells were washed, lysed with sterile water at 37°C for 30’ and serially diluted 1:10 to be seeded for CFU count. Alternatively, cells were incubated with 10% AlamarBlue solution for 2 hr for the viability assays.

THP-1 Monocyte

Based on their responses to stimuli, *in vivo* macrophages can be classified into two main activation states: M1 and M2.

M1 macrophages, or classically activated macrophages, are primarily involved in defending against bacterial and viral infections and in tumor regression. The M1 phenotype is induced from resting macrophages upon exposure to pathogen-associated molecular patterns (PAMPs) or Th1 cytokines, such as interferon-gamma (IFNγ) and tumor necrosis factor-alpha (TNFα). They are characterized by the high production of pro-inflammatory cytokines, including TNFα, interleukin (IL)-1β, IL-6, IL-8, and IL-12. They also express pattern recognition receptors (PRRs), such as Toll-like receptors (TLRs) and NOD-like receptors (NLRs), which enable them to recognize and respond to pathogens.

M2 macrophages, or alternatively activated macrophages, play essential roles in parasite infections, tissue remodeling, immunoregulation, allergy, and tumor progression. M2 macrophages are derived from resting macrophages upon stimulation by Th2 cytokines, such as IL-4 and IL-13. These macrophages exhibit an anti-inflammatory profile associated with wound healing and tissue repair.

The M1 and M2 macrophage polarization reflects the functional diversity of macrophages in various immune responses and disease contexts.

THP-1 cells (ATCC® TIB-202™) are a spontaneously immortalized monocyte-like line derived from the peripheral blood of a child with acute monocytic leukemia. This cell line is widely used to investigate monocyte/macrophage functions, signaling pathways, and nutrient and drug transport mechanisms. It serves as a reliable model for studying the modulation of monocyte and macrophage activities. THP-1 cells grow in suspension at 37°C and 5% CO_2. They are grown in RPMI 1640 medium supplemented with Hepes, L-glutamine, glucose, sodium pyruvate, and 10% fetal bovine serum (FBS). Cells were kept between 0.5 and 1x106 cells/ml in a ventilated 75 cm^2 flask for a

maximum of 18 passages until seeded. Cells were counted using a Bürker's chamber after staining with 0.4% Trypan Blue solution, which stains dead cells, enabling the distinction of viable (unstained) and dead (blue-stained) cells under a microscope.

For infection experiments, 5.5×10^5 THP-1 cells were plated in a Tissue cultures treated 96-well plate in presence of 100 nM Phorbol 12-Myristate 13-Acetate (PMA) to induce the differentiation. PMA treatment was performed for 3 days at 37°C, followed by 2 days of rest to obtain M0-like phenotypes. Macrophages were also polarized to an M1-like and M2-like phenotype with, respectively, 50 ng/mL LPS and 20 ng/mL IL-4 for 16 hours. Experiments were carried out with the three different phenotypes.

Infection was carried out using H37Rv_mCHERRY at an exponential growth phase (OD_{600}: 0.4–0.6) with a multiplicity of infection (MOI) of 5:1. The infected plates were centrifuged at 300 × g for 5 minutes at room temperature to facilitate contact with macrophages. After 2 hours, extracellular bacteria were removed. After 24 and 72 hr, cells were washed, lysed with sterile water at 37°C for 30' and serially diluted 1:10 to be seeded for CFU count. Alternatively, cells were incubated with 10% AlamarBlue solution for 2 hr for the viability assays.

Nicotine's treatment

This first sets of experiments was conducted to establish the Nicotine concentration and incubation times.

Nicotine solution (Sigma, [+/-]-Nicotine - n0267) has been stocked at 4°C. Stock solutions were prepared according to manufacturer instruction by diluting nicotine in EtOH to 100 mM.

The concentrations used to treat the cells were selected according to the literature, and the same applies to the evaluated time points.

The concentrations and time points tested are shown in Table 2.

Table 2. Schematic representation of the different nicotine's concentrations and of the various time points that have been selected.

Nicotine's concentrations	**Timepoints of evaluation**
100 μM	24 hours
40 μM	48 hours
20 μM	72 hours
10 μM	5 days
5 μM	6 days
1 μM	
0,1 μM	

For nicotine treatment, adherent cells were detached from the plastic surface with the appropriate enzyme, counted and seeded at $2{,}5 \times 10^4$ cells/well.

Pre-warmed, cell-specific media were enriched with nicotine to reach the highest desired concentration (100 μM). Serial dilutions were then performed to obtain the other concentrations (Table 1). EtOH-enriched media were prepared by adding a volume of EtOH equivalent to that used for the highest desired nicotine concentration (100 μM).

Cells were allowed to adhere and grow for 24 hours before treatment. Then, the culture medium was substituted with the nicotine-containing medium. Untreated cells and EtOH-treated cells were used as growth controls.

After 24 hours, 48 hours, 72 hours, 5 and 6 days of incubation, cells were incubated with a 10% AlamarBlue solution for 2 hours for the viability assays.

Viability assay

The AlamarBlue assay is a widely used method for assessing cell viability. It is valued for its simplicity, non-toxic nature, and reliability in prokaryotic and eukaryotic cells. The assay is based on metabolic enzymes such as FAD and NAD reducing the blue, non-fluorescent molecule resazurin, into resorufin, a pink, highly fluorescent compound. This reduction correlates directly with cellular metabolic activity.

Following the manufacturer's instructions, 50 µL of a 10x AlamarBlue solution (prepared at 0.2% in DPBS and sterilized using a 0.22 µm filter system) was added to each well containing 500 µL of medium. The plates were then incubated for 2 hours in the dark at 37°C with 5% CO_2.

After incubation, 100 µL of medium from each well was transferred to a 96-well black plate. Fluorescence was measured using a Perkin Elmer Victor X4 Multilabel Microplate Reader with excitation/emission filter settings of 560/590 nm.

Mtb H37Rv_ mCHERRY infection

H37Rv_mCHERRY was grown to a maximum OD_{600} of 0.6, corresponding to the empirical end of the logarithmic growth phase.

To measure the OD, 900 µL of the culture was inactivated by adding 100 µL of 37% formaldehyde directly into a cuvette. After 30 minutes of inactivation, the OD was measured using a spectrophotometer set to 600 nm. The OD value was used to determine the bacterial concentration in the culture; for the Mtb strain, an OD_{600} value of 1 corresponds to 10^8 mycobacteria/mL.

The calculated volume of the H37Rv_mCHERRY culture was centrifuged at 13,000 rpm for 7 minutes and washed twice with DPBS. The resulting pellet was resuspended in 1 mL of cell-specific medium, and clumps were dispersed by

repeatedly passing the suspension through a 26/27-gauge needle. The resulting homogeneous bacterial suspension was then appropriately diluted in a cell-specific medium.

The prepared bacterial suspension subsequently replaced the host cells medium for approximately 16 hours (overnight) at 37°C with 5% CO2,

At each time point, both viability assay and CFU count were performed (Figure 7).

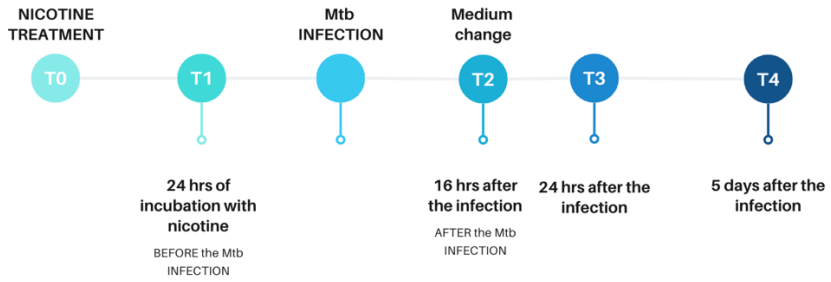

Figure 7. Schematic representation of the sampling timeline.

The infection with Mtb H37Rv_mCHERRY was optimized using three different infection protocols for the LF-hTERT and HBEC-3kt cell lines. The protocols differed in the adhesion and replication times of the cells, the exposure duration to nicotine, and whether the infection was performed in the presence or absence of nicotine. Each protocol was designed to evaluate the influence of nicotine on Mtb infection dynamics under varying cellular conditions and are better depicted above:

Protocol 1

The first protocol follows the steps described below:

Cell Preparation

- Seed 5000 cells per well in 24-well plates and allow overnight adhesion.
- Treat cells with two nicotine concentrations (1 μM and 40 μM) after washing with PBS and replacing the medium.

Bacterial Preparation (M. tuberculosis H37Rv_mCHERRY)

- A logarithmic-phase culture was used to grow in the Middlebrook 7H9 medium.
- Inactivate aliquots with formaldehyde for OD_{600} measurement and calculate the MOI (100:1).
- Prepare the bacterial suspension in an antibiotic-free medium for infection.

Cell Infection

- Remove the nicotine-containing medium, wash with PBS, and add the bacterial suspension to the wells.
- Incubate the infected cells at 37°C in a CO_2 atmosphere overnight.
- Wash with PBS to remove non-internalized bacteria and replace with fresh, antibiotic-free medium.

Protocol 2

In the second protocol setting, cells were allowed to adhere for 72 hours before nicotine treatment. Mtb infection was carried out in the presence of nicotine.

The second protocol follows the steps described below:

Cell Preparation

- Seed 5000 cells per well in 24-well plates, allowing over 72 hours of adhesion.
- Treat cells with two nicotine concentrations (40 μM) after washing with PBS and replacing the medium.

Bacterial Preparation (M. tuberculosis H37Rv_mCHERRY)

- A logarithmic-phase culture was used to grow in the Middlebrook 7H9 medium.
- Inactivate aliquots with formaldehyde for OD_{600} measurement and calculate the MOI (100:1).
- Prepare the bacterial suspension in an antibiotic-free medium for infection.

Cell Infection

- Remove the nicotine-containing medium, wash with PBS, and add the bacterial suspension to the wells.
- Incubate the infected cells at 37°C in a CO_2 atmosphere overnight.
- Wash with PBS to remove non-internalized bacteria and replace with fresh, antibiotic-free medium.

Protocol 3

This third protocol follows the abovementioned steps, increasing the seeding density (20,000 cells/well) to ensure confluence before nicotine treatment and infection. Moreover, the infection was performed in this case, and the nicotine supplement was maintained in the medium. Ultimately, only one nicotine concentration was selected according to the previous data obtained from the other two protocols.

Cell Preparation

- Seeding: Seed 5000 cells per well in a 24-well plate, allowing cells to reach confluence over the weekend.
- Preparation for Cotreatment:
    - Remove the medium and wash the wells twice with PBS.
    - Add 500 µL of medium (without antibiotics) prepared with ethanol (0.04%) or nicotine (40 µM).

Bacterial Preparation (M. tuberculosis H37Rv_mCHERRY)

- A logarithmic-phase culture was used to grow in the Middlebrook 7H9 medium.
- Inactivate aliquots with formaldehyde for OD_{600} measurement and calculate the MOI (100:1).
- Prepare the bacterial suspension in an antibiotic-free medium for infection.

Cell Infection

- Remove the nicotine-supplemented medium, collect for storage (-80°C), and add 500 µL of bacterial suspension at MOI 100:1.
- Incubate infected cells overnight at 37°C in a CO_2 atmosphere.

CFU Count - Direct Plating Method

Colony Forming Unit (CFU) counts are used to quantify the number of viable bacteria in a sample. To perform CFU counting, bacterial suspensions are serially diluted in PBS, and 50 µL of each dilution is spread onto agar plates (Middlebrook 7H10).

The inoculated agar plates are incubated at 37°C in a CO_2-enriched atmosphere for 21 days. After incubation, colonies are counted to determine the number of viable bacteria per mL in each dilution and subsequently in the original culture. At each time point, cells were lysed to release intracellular bacteria. HBEC3-KT cells were lysed in 500 μL of 0.5% SDS, while hTERT-HLF and THP-1 cells were lysed in 500 μL and 100 μL of distilled water, respectively.

The lysates from infected cells were collected, and the number of viable mycobacteria was quantified using CFU counts.

Bioink Preparation and 3D Hydrogel Scaffold Fabrication

HBEC3-KT, hTERT-HLF, and THP-1 cells were utilized to create a granuloma-like model comprising an outer layer (shell) and a core. Cells were counted, centrifuged at 1200 RPM for 5 minutes (HBEC and HLF) or at 1800 RPM for 8 minutes (THP-1), and resuspended in a 1:10 medium-to-hydrogel ratio. Using two Luer-lock syringes, HBECs were mixed with CELLINK Bioink to form the shell, while HLFs and THP-1 cells were mixed with CELLINK Laminink 411 (CELLINK AB, Gothenburg, Sweden) to constitute the core.

Several preliminary seeding and printing attempts were conducted to determine the required cell concentrations (data not shown). The 3D scaffold was designed to have a total size of 4×4×4 mm, with a core measuring 2×2×2 mm. Based on these preliminary experiments, the cell concentrations were adjusted to 7×10^7 THP-1 cells/mL and 4×10^6 HLF cells/mL in GelXA Laminink 411 for the core and 2×10^6 HBEC cells/mL in GelMA Fibrin for the shell (10 models/ml).

The cell-laden bioinks were transferred into cartridges and loaded onto a Bio X 3D bioprinter (CELLINK AB, Gothenburg, Sweden). Scaffold designs were developed using Fusion360 (Autodesk) and prepared for printing using the Bio X slicer software. The slicing process employed a rectilinear infill pattern with 30%

density. Printing was conducted using a 22G (410 μm diameter) nozzle at a deposition speed of 5 mm/s, with the bioprinting environment maintained at 22°C.

Following printing, the constructs were subjected to a dual crosslinking process. Initial UV crosslinking was performed at 405 nm for 15 seconds, followed by ionic crosslinking in a 50 mM $CaCl_2$ solution (CELLINK AB, Gothenburg, Sweden) for 4 minutes at room temperature. Per the manufacturer's instructions, the scaffolds were washed once with Hank's Balanced Salt Solution (HBSS; EuroClone, Pero, Italy) to remove residual crosslinking agents.

The constructs were submerged within 30 minutes of fabrication in a complete keratinocyte serum-free medium (KSFM; Thermo Fisher Scientific, Milan, Italy) to maintain cell viability. The scaffolds were subsequently incubated at 37°C in a 5% CO_2 atmosphere and maintained for downstream analyses.

After stabilization, the models were treated with phorbol 12-myristate 13-acetate (PMA) at a final concentration of 25 ng/mL for 72 hours to induce the differentiation of THP-1 cells in the core of the models into macrophages. Following the differentiation period, the models were washed twice with DPBS, with each wash lasting 10 minutes. The medium was then replaced with pre-warmed KSFM and incubated for an additional 72 hours to allow the macrophages to stabilize during the "rest" phase.

The models were incubated with either nicotine (40 μM) or EtOH (0.013%) for 72 hours at 37°C in a 5% CO_2 atmosphere. Simultaneously, two H37Rv_mCHERRY cultures were prepared as previously described, adjusted to a final concentration of 10^7 cells/mL, and pretreated with either nicotine (40 μM) or EtOH (0.013%) under the same conditions for 72 hours at 37°C. After the pretreatment, the medium in the models was replaced with 1 mL of the

corresponding H37Rv_mCHERRY pretreated suspension (MOI 5:1), and the models were incubated for 3 and 10 days at 37°C in a 5% CO_2 atmosphere.

At each time point, the viability of the 3D bioprinted models was assessed using the LIVE/DEAD® Cell Imaging Kit (Thermo Fisher Scientific, Massachusetts, USA), which enables the visualization of live cells (Calcein AM, green) and nuclei (NuncBlue, blue).

Scaffolds were washed twice with DPBS for 10 minutes and then incubated with the Live/Dead reagent, prepared as a 1:1000 dilution of Calcein AM and 3 drops of NuncBlue in 1 mL of KSFM. After a 2-hour incubation at 37°C in a 5% CO_2 atmosphere, the models were washed twice more with DPBS for 10 minutes and inactivated overnight in 4% formaldehyde in PBS at 4°C.

The models were washed twice with DPBS for 10 minutes and imaged using a Confocal Olympus FluoVIEW 3000 RS microscope equipped with appropriate filters. Images were acquired using Olympus software, exported, and analyzed with FIJI (ImageJ).

To perform CFU counting, three models were collected at each time point, cut into small pieces using a scalpel, and each transferred to Eppendorf tubes containing 1 mL of enzymatic dissolution buffer. The buffer was prepared by dissolving 0.01 g of Dispase II, 0.005 g of DNase, 0.005 g of Papain, and 0.03057 g of $MgSO_4$ in 10 mL of distilled water. The samples were homogenized for 3 minutes using a TissueLyser to enhance mechanical dissociation. After 30 minutes, the solution was filtered through 70 μm cell strainers to remove debris and washed with 9 mL of DPBS. The resulting cell suspension was centrifuged at 2700 × g for 10 minutes, and the pellet was lysed in 5 mL of sterile water overnight. Lysates from the infected models were collected, and viable mycobacteria were quantified through CFU counting.

Statistical analysis

Statistical analyses were performed using GraphPad Prism software (version 10.2.3). Data are presented as mean ± standard deviation (SD) from at least three independent experiments. Differences between groups were assessed using a two-tailed Student's t-test for independent samples. A p-value < 0.05 was considered statistically significant.

Chapter 5: Results

The findings of this study highlight the significant impact of nicotine-induced oxidative stress on Mtb infection dynamics within a 3D lung model. The increased susceptibility of epithelial and immune cells to infection under oxidative stress conditions suggests a potential mechanism by which smoking exacerbates TB pathogenesis. This observation aligns with epidemiological data linking cigarette smoking with increased TB incidence, prolonged disease progression, and poorer treatment outcomes.

From a clinical standpoint, these results emphasize the need for targeted therapeutic strategies addressing oxidative stress and its role in TB progression. Current TB treatments primarily focus on antimicrobial therapy. Still, these findings suggest that integrating antioxidant-based therapies or nicotinic receptor modulators could improve host resistance, especially in populations with high smoking prevalence. Moreover, therapies designed to restore epithelial barrier integrity—such as tight junction stabilizers or anti-inflammatory agents—could reduce pathogen entry and colonization in the lung microenvironment.

Beyond TB, this study has broader implications for other pulmonary infectious diseases where oxidative stress contributes, including chronic obstructive pulmonary disease (COPD)-associated bacterial infections and viral respiratory diseases. Given that nicotine exposure is linked to increased severity of infections such as COVID-19 and influenza, this research underscores the importance of understanding how environmental and behavioral factors contribute to lung vulnerability.

Additionally, precision medicine approaches could leverage these findings by identifying patient subgroups that would benefit from adjunctive antioxidant or immune-modulating therapies. Smoking cessation programs,

already a key component of TB prevention strategies, could be reinforced by mechanistic insights into how nicotine exposure worsens infection outcomes.

Effect of Nicotine Treatment on Cell Viability

LF-hTERT Fibroblasts

The first set of experiments evaluated the response of each cell line used in this thesis to nicotine. The main aim is to determine the optimal concentrations and time points to simulate chronic exposure while maintaining cell viability and avoiding cytotoxicity.

The colorimetric AlamarBlue assay was conducted daily over a 6-day culture period to evaluate the viability of each cell line exposed to varying nicotine concentrations (0.1–100 μM). Data were normalized to control wells treated with an ethanol (EtOH) concentration equivalent to that present in the highest nicotine concentration.

For the LF-hTERT cell line, 5 independent experiments were performed.

Data showed that at 24 hours, cell viability decreased proportionally with increasing nicotine concentrations. No significant difference was observed between the two groups (Figures 8a and 8b). Moreover, this trend was not sustained after the 24-hour evaluation: the viability reduction appeared to attenuate with prolonged incubation due to cellular overcrowding and nutrient depletion within the multiwell culture system. The experimental setup may diminish nicotine's direct effects, as evidenced by the altered metabolic activity detected via the AlamarBlue assay at subsequent time points beyond 24 hours.

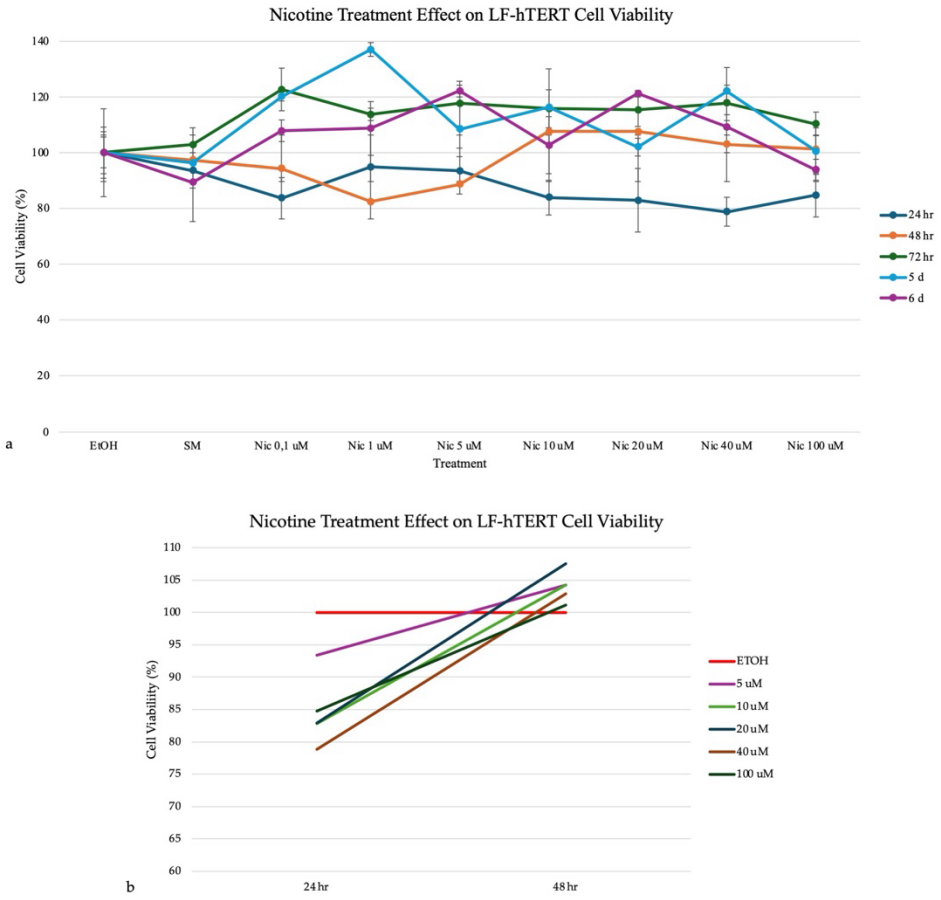

Figure 8. Graph (a) represents the cell viability of LF-hTERT cells treated with different nicotine concentrations. Data were obtained using the AlamarBlue assay after 24 hours, 48 hours, 72 hours, 5 and 6 days, and normalized to the untreated control (100% viability). The untreated control consists of cells cultured in standard medium (SM) supplemented with the highest ethanol (EtOH) concentration present in the nicotine dilutions (100 uM). Graph (b) reported only the most valuable time points (24 and 48 hours) to better highlight the results obtained. Values represent the mean ± standard deviation (SD) from at least three independent experiments. $p < 0.05$ indicates a statistically significant difference compared to the control. In graph (b), SDs are not reported to make the graph more readable, but the SDs refer to the same as those reported in graph (a).

HBEC-3kt Bronchial Epithelial Cells

The colorimetric AlamarBlue assay was conducted after 24 and 48 hours to evaluate the viability of each cell line exposed to two nicotine concentrations: 1 µM (threshold effect) and 40 µM (maximum effect). Data were normalized to control wells treated with an ethanol (EtOH) concentration equivalent to that present in the highest nicotine concentration.

For the HBEC-3kt cell line, 3 independent experiments were performed. The results showed a concentration-dependent decrease in cell viability at both time points (Figure 9). No significant difference was detected between the nicotine and control groups.

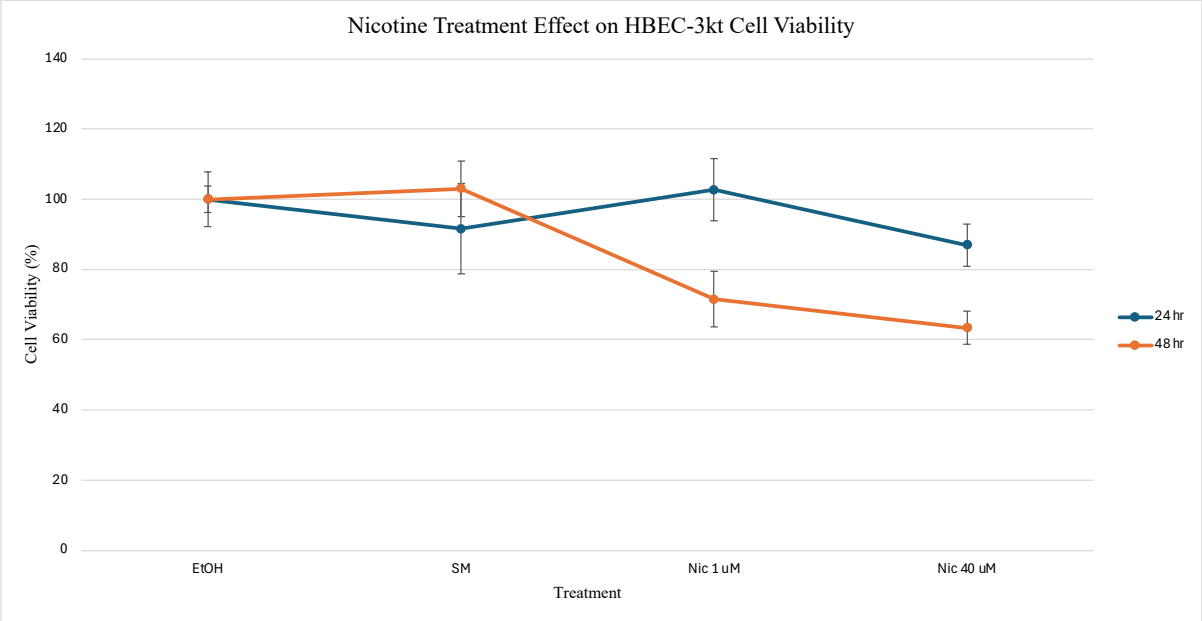

Figure 9. The graph represents the cell viability of HBEC-3kt cells treated with different nicotine concentrations. Data were obtained using the AlamarBlue assay after 24 and 48 hours and normalized to the untreated control (100% viability). The untreated control consists of cells cultured in standard medium (SM) supplemented with the highest ethanol (EtOH) concentration present in the nicotine dilutions (40 uM). Values represent the mean ± standard deviation (SD)

from at least three independent experiments. $p < 0.05$ indicates a statistically significant difference compared to the control.

THP-1 Monocyte Cells

The colorimetric AlamarBlue assay was conducted after 24 and 72 hours to evaluate the viability of each cell line exposed to nicotine 40 μM (maximum effect). Data were normalized to control wells treated with an ethanol (EtOH) concentration equivalent to that present in the highest nicotine concentration.

For the THP-1 cell line, 3 independent experiments performed.

The results showed a concentration-dependent decrease in cell viability at both time points, with no significant differences observed between the nicotine-exposed and control groups (Figure 10).

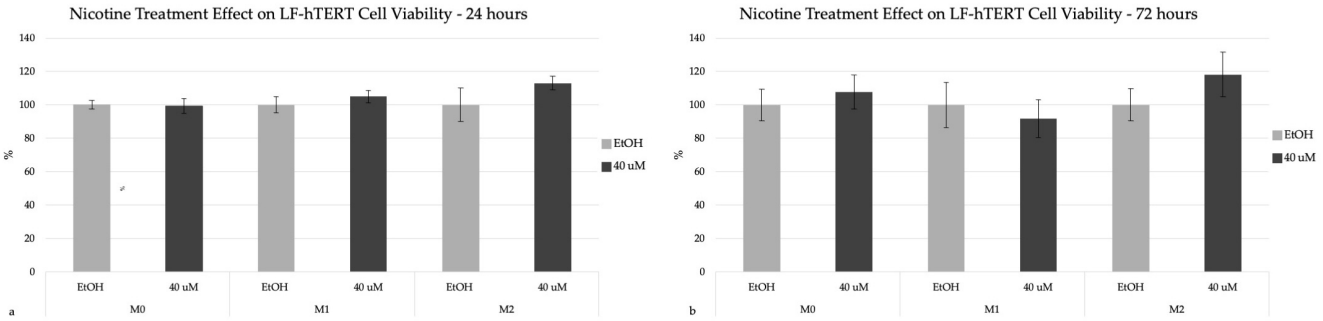

Figure 10. The graph represents the cell viability of HBEC-3kt cells treated with different nicotine concentrations. Data were obtained using the AlamarBlue assay after 24 and 48 hours and normalized to the untreated control (100% viability). The untreated control consists of cells cultured in standard medium (SM) supplemented with the highest ethanol (EtOH) concentration present in the nicotine dilutions (40 uM). Values represent the mean ± standard deviation (SD) from at least three independent experiments. $p < 0.05$ indicates a statistically significant difference compared to the control.

Effect of Nicotine Treatment on *Mycobacterium Tuberculosis* Infection

Infection with *Mycobacterium tuberculosis* H37Ra

This set of experiments aimed to assess the Mtb infection dynamics in LF-hTERT and HBEC-3kt cell lines, which are not commonly used for studying tubercular infection. The initial protocol assessment was performed with the less virulent Mtb strain known as H37Ra.

To assess the impact of nicotine on Mtb infection, both LF-hTERT and HBEC-3kt cells were infected with Mtb H37Ra (MOI 100:1). Cells were pre-treated with nicotine (1 μM or 40 μM), and subsequently infected. Cell viability was evaluated using AlamarBlue staining 24 hours and 5 days after the infection. At 24 hours post-infection, nicotine-treated and non-infected LF-hTERT cells showed lower viability than untreated cells, particularly at 40 μM. In contrast, once both cell lines have been nicotine-treated and infected, they exhibited higher viability, with a non-linear progression, unlike previous experiments. After 5 days from the infection, on the contrary, the nicotine effect reported is more linear within the different cell lines and considering the different concentrations (results are reported in Figure 11a for the 24 hours and in Figure 11b for the 5 days). The graph in Figure 11c compares cell viability between infected and non-infected cells for the LF-hTER and HBEC-3kt cell lines at the first time point.

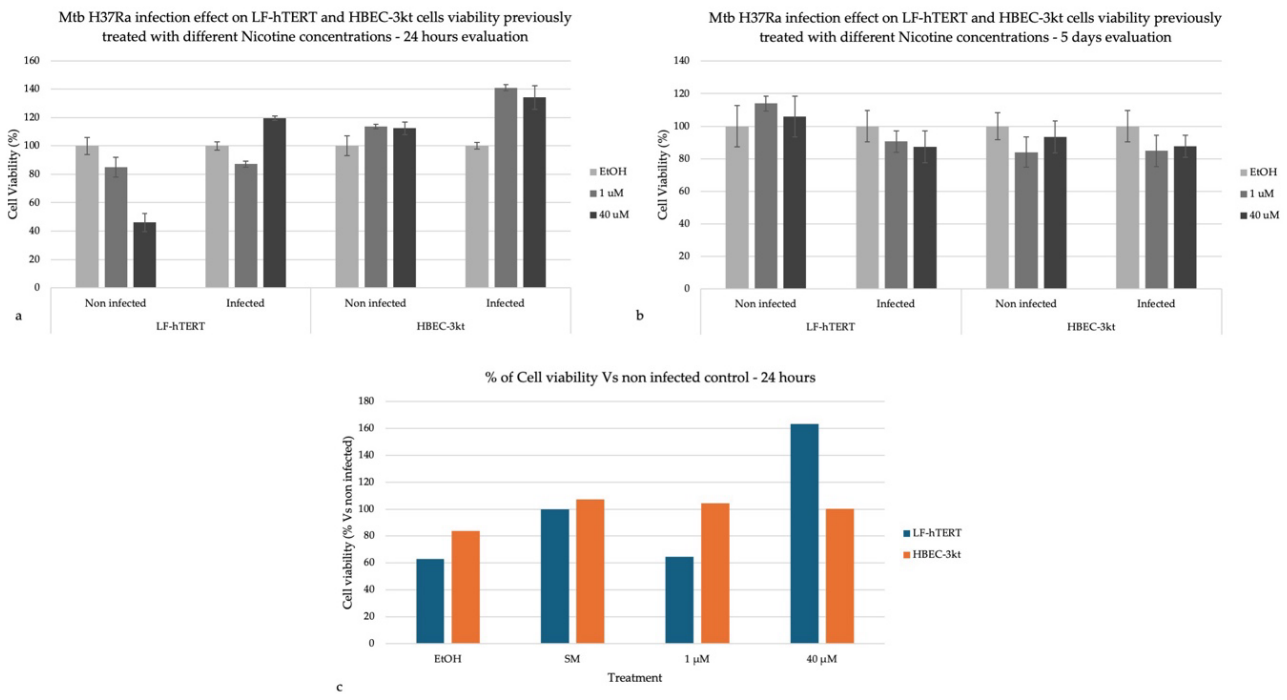

Figure 11. The graph represents the cell viability of LF-hTERT and HBEC-3kt cells treated with two nicotine concentrations (1 µM or 40 µM). Data were obtained using the AlamarBlue assay after 24 hours (a) and 5 days (b) from the Mtb H37Ra infection and normalized to the untreated control (100% viability). The untreated control consists of cells cultured in a standard medium supplemented with the highest ethanol (EtOH) concentration in the nicotine dilutions (40 uM). Values represent the mean ± standard deviation (SD) from at least three independent experiments. $p < 0.05$ indicates a statistically significant difference compared to the control. Graph (c) represents the diversity in the cell viability (expressed as %) obtained by comparing infected vs non-infected (control) cells.

These results suggest that nicotine exposure, in combination with infection, may alter the cell's response, highlighting a potential immunomodulatory effect of nicotine during Mtb infection. However, the data are not entirely linear, which could be associated with using a less virulent strain.

Infection with *Mycobacterium tuberculosis* H37Rv_mCHERRY on LF-hTERT and HBEC-3kt cell lines

In this series of experiments, as well as in the subsequent ones, infections were performed using fluorescent mutant strains derived from the laboratory reference strain H37Rv, designated as H37Rv_mCHERRY.

To assess nicotine's impact on tuberculosis infection, LF-hTERT and HBEC-3kt cells were infected with Mtb H37Rv_mCHERRY (MOI 100:1). The infection was carried out following three different protocols for the LF-hTERT and the HBEC-3kt cell lines to set the best one as described in the Material and Methods section.

Cell viability was evaluated using AlamarBlue assay. Mtb growth was assessed using the CFU counting methods. Only one time point has been selected for the evaluation (24 hours).

The Alamar blue assay results and the CFU counts are reported in Figures 12 and 13, respectively.

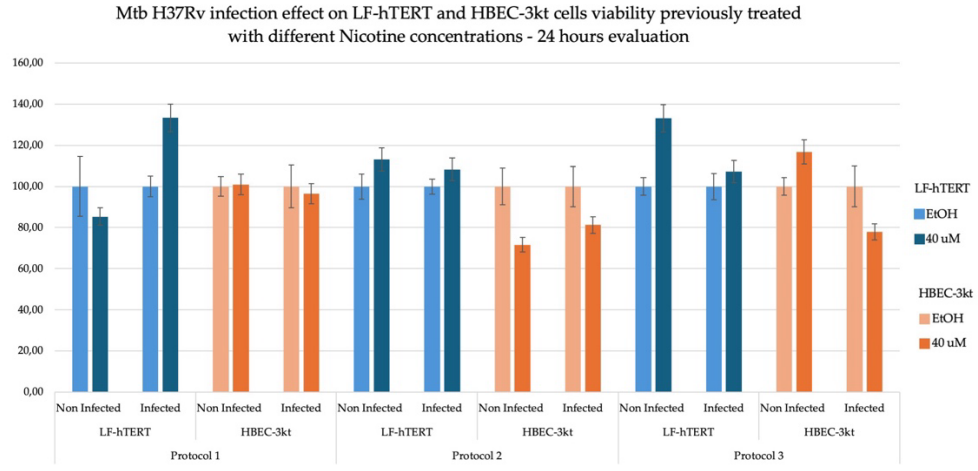

Figure 12. The graph represents the cell viability of LF-hTERT and HBEC-3kt cells treated with one nicotine concentration (40 μM). Data were obtained using the AlamarBlue assay and normalized to the nicotine-untreated control (100% viability). The untreated control consists of cells cultured in a standard medium supplemented with the highest ethanol (EtOH) concentration in the nicotine dilutions (40 uM). Values represent the mean ± standard deviation (SD) from at least three independent experiments. $p < 0.05$ indicates a statistically significant difference compared to the control.

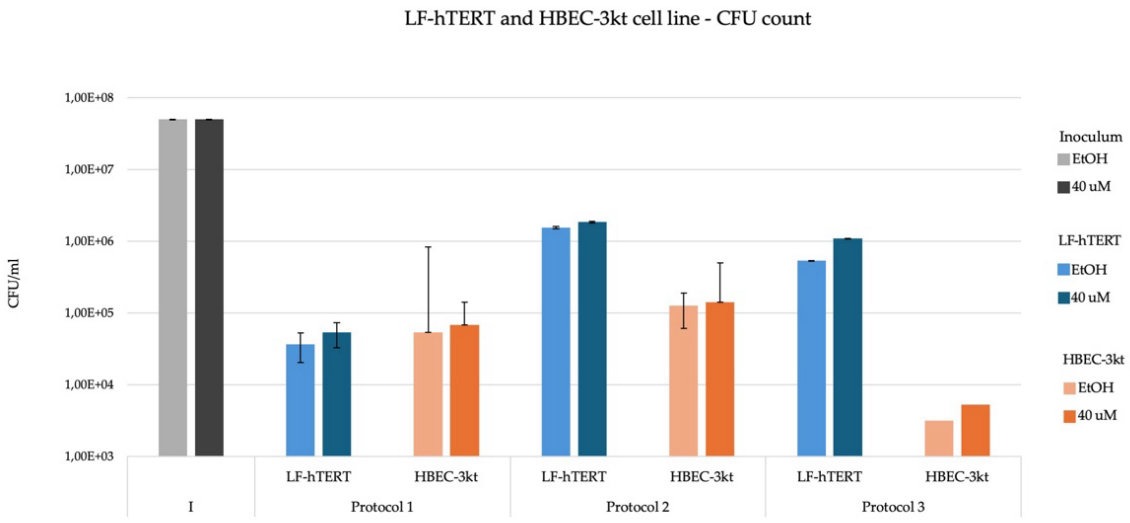

Figure 13. The graph represents the CFU counts of Mtb H37Rv_mCHERRY recovered from LF-hTERT and HBEC-3KT cells treated with one nicotine concentration (40 μM) following the three protocols already described in the Material and Methods section. Data were normalized to inoculum (CFU counts set as 100%). The untreated control for the nicotine treatment consists of cells cultured in a standard medium supplemented with the highest ethanol (EtOH) concentration in the nicotine dilutions (40 uM). Values represent the mean ± standard deviation (SD) from at least three independent experiments. $p < 0.05$ indicates a statistically significant difference compared to the control.

The data obtained show cell viability in the control group (EtOH) and in response to nicotine treatments (40 uM), both in the presence and absence of Mtb

infection in LF-hTERT and HBEC-3kt cell lines. In the control group, the viability of non-infected cells remains more or less stable, which is more expected since the evaluation was performed 72 hours after cell seeding. On the contrary, it decreases in infected cells.

These results suggest that nicotine exposure, in combination with infection, may alter the cell's response, highlighting a potential immunomodulatory effect of nicotine during Mtb infection.

Regarding CFU, nicotine treatment consistently and steadily increases cellular growth, although it is not statistically significant in both cell lines.

Infection with *Mycobacterium tuberculosis* H37Rv_mCHERRY on THP-1 cell line

In this set of experiments, we aimed to assess the role of nicotine pre-exposure on the capability of macrophages to counteract Mtb infection.
Infections were carried out with H37Rv_mCHERRY applying Protocol 3 (previously described in the Materials and Methods section).

THP-1 cells were infected with Mtb H37Rv_mCHERRY (MOI 5:1) to assess nicotine's impact on tubercular infection. Two time points were considered: 24 and 72 hours. Additionally, polarization into M1 and M2 phenotypes was performed for this cell line before nicotine treatment and infection, as described in the Material and Methods section. Cell viability was evaluated using AlamarBlue assay (Figure 14a for the 24 hours time point and Figure 14b for the 72 hours time point), and Mtb growth was assessed using the CFU counting method (Figure 15).

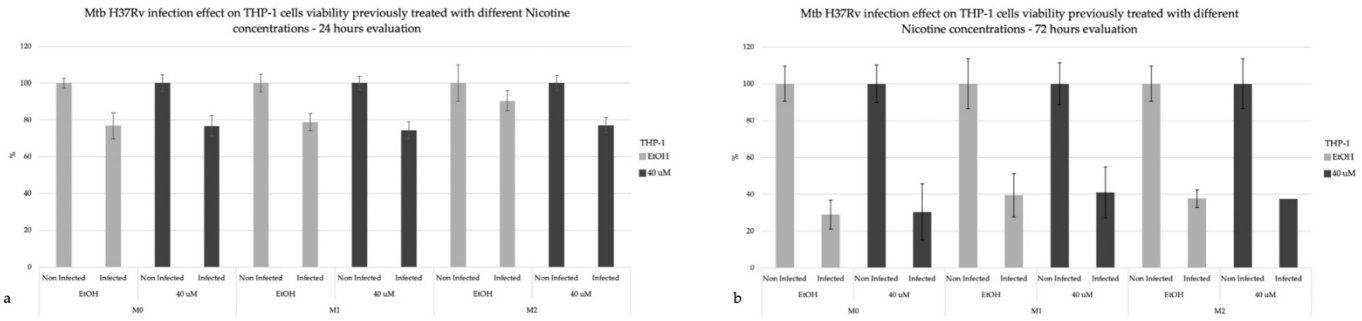

Figure 14. The graph represents the cell viability of THP-1 cells treated with one nicotine concentration (40 μM). Data were obtained using the AlamarBlue assay after 24 (a) and 72 (b) hours from Mtb H37Rv_mCHERRY infection and normalized to the nicotine-untreated control (100% viability). The untreated control consists of cells cultured in a standard medium supplemented with the highest ethanol (EtOH) concentration in the nicotine dilutions (40 uM). Values represent the mean ± standard deviation (SD) from at least three independent experiments. $p < 0.05$ indicates a statistically significant difference compared to the control. In particular, graph (a) represents the diversity in the cell viability (expressed as %) obtained by comparing cells previously exposed to nicotine vs non-exposed cells. Graph (b) represents the diversity in the cell viability (expressed as %) obtained by comparing infected vs non-infected cells.

The data obtained show cell viability (%vit) in the control group (EtOH 0.013%) and in response to treatments with nicotine (40 uM), both in the presence and absence of Mtb infection. In the control group, the viability of non-infected cells remained at 100%. On the contrary, it significantly decreased in infected cells. The addition of nicotine affected cell viability differently; specifically, in the infected cells, data shows a decrease in viability in M1 and M2 conditions, suggesting a potential negative impact on the cell's response to infection.

These results suggest that nicotine exposure, in combination with infection, may alter the cell's response, highlighting a potential immunomodulatory effect of nicotine during Mtb infection.

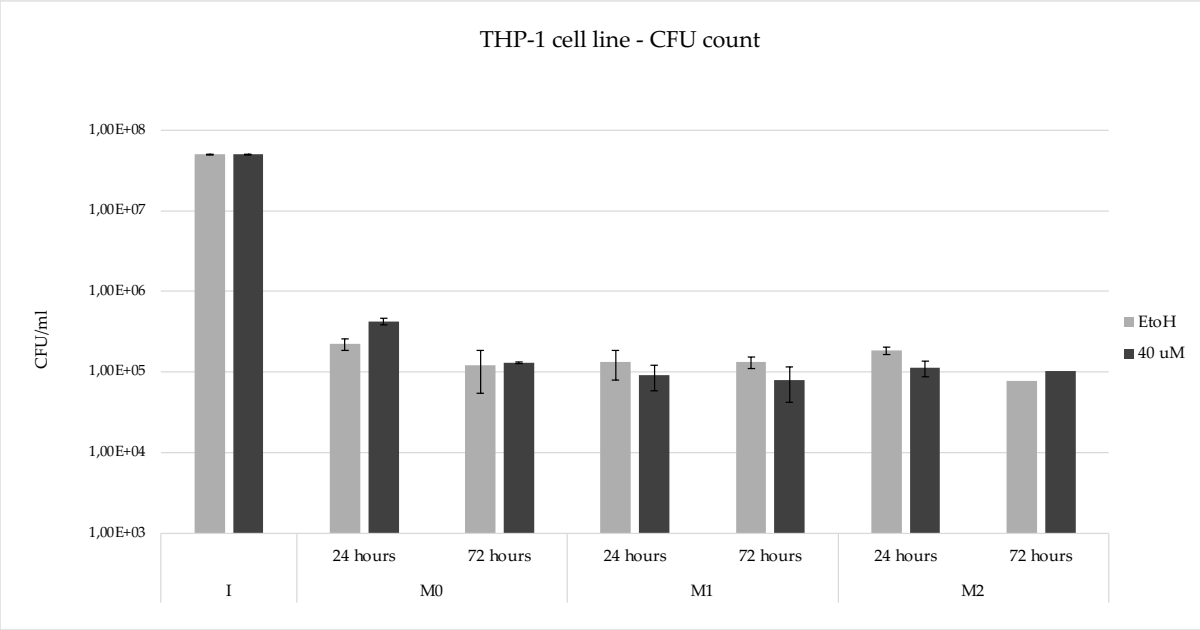

Figure 15. The graph represents the CFU counts of Mtb H37Rv_mCHERRY recovered from THP-1 cells treated with one nicotine concentration (40 μM). CFU quantification was performed 24 hours after the Mtb H37Rv_mCHERRY infection. Data were obtained using the AlamarBlue assay after 24 hours of simultaneous nicotine treatment and Mtb H37Rv_mCHERRY infection. Data were normalized to inoculum (CFU counts set as 100%). The untreated control for the nicotine treatment consists of cells cultured in a standard medium supplemented with the highest ethanol (EtOH) concentration in the nicotine dilutions (40 μM). Values represent the mean ± standard deviation (SD) from at least three independent experiments. $p < 0.05$ indicates a statistically significant difference compared to the control.

The data reported above confirm that nicotine exposure significantly increased bacterial growth in the M0 model. The total CFU/ml was $4.27 \times 10^{5,}$ nearly double the CFU/ml evaluated in the control condition. However, the effect

of NIC was less pronounced in the M1 and M2 conditions. In particular, in the control group, there was a decrease in CFU/ml over time, from 24 hours to 72 hours, particularly for M1 and M2. In contrast, the nicotine-treated group showed a relatively stable bacterial growth pattern over time, with only slight reductions in CFU/ml in M0 and M2, while M1 demonstrated a substantial drop. These results indicate that nicotine exposure tends to promote bacterial growth over time.

Infection with *Mycobacterium tuberculosis* H37Rv_mCHERRY on the 3D model

The 3D model used in this experiment is a granuloma-like model composed of three cell lines: HBEC3-KT (human bronchial epithelial cells), hTERT-HLF (human lung fibroblasts), and THP-1 (human monocytic cells). This model was designed to mimic the pulmonary microenvironment, providing a more accurate representation of the interactions between host cells and Mtb than traditional 2D cultures. The model was 3D printed using CELLINK Bioink for the outer shell of the granuloma (HBEC3-KT cells) and CELLINK Laminink 411 for the inner core (hTERT-HLF and THP-1 cells). After cross-linking and infection with Mtb H37Rv, the model was used to assess bacterial growth and host response over time, allowing for the evaluation of factors such as nicotine exposure in the context of tuberculosis infection. This approach offers a more physiologically relevant platform for studying infection dynamics and immune responses.

The main results were obtained through confocal microscopy analysis. Notably, three days post-infection, the main difference observed was that in the nicotine-treated model, bacteria were found even in the central portion of the granuloma (Figure 16), whereas, in the ethanol-treated model, very few bacteria were present in the core, with a higher number trapped in the outer epithelial

layer (granuloma shell - refer to attached Z-stack images). This suggests that nicotine exposure facilitates the breach of the epithelial barrier, enabling easier spread within the granuloma structure. This, in turn, may promote the dissemination of Mtb within the granuloma.

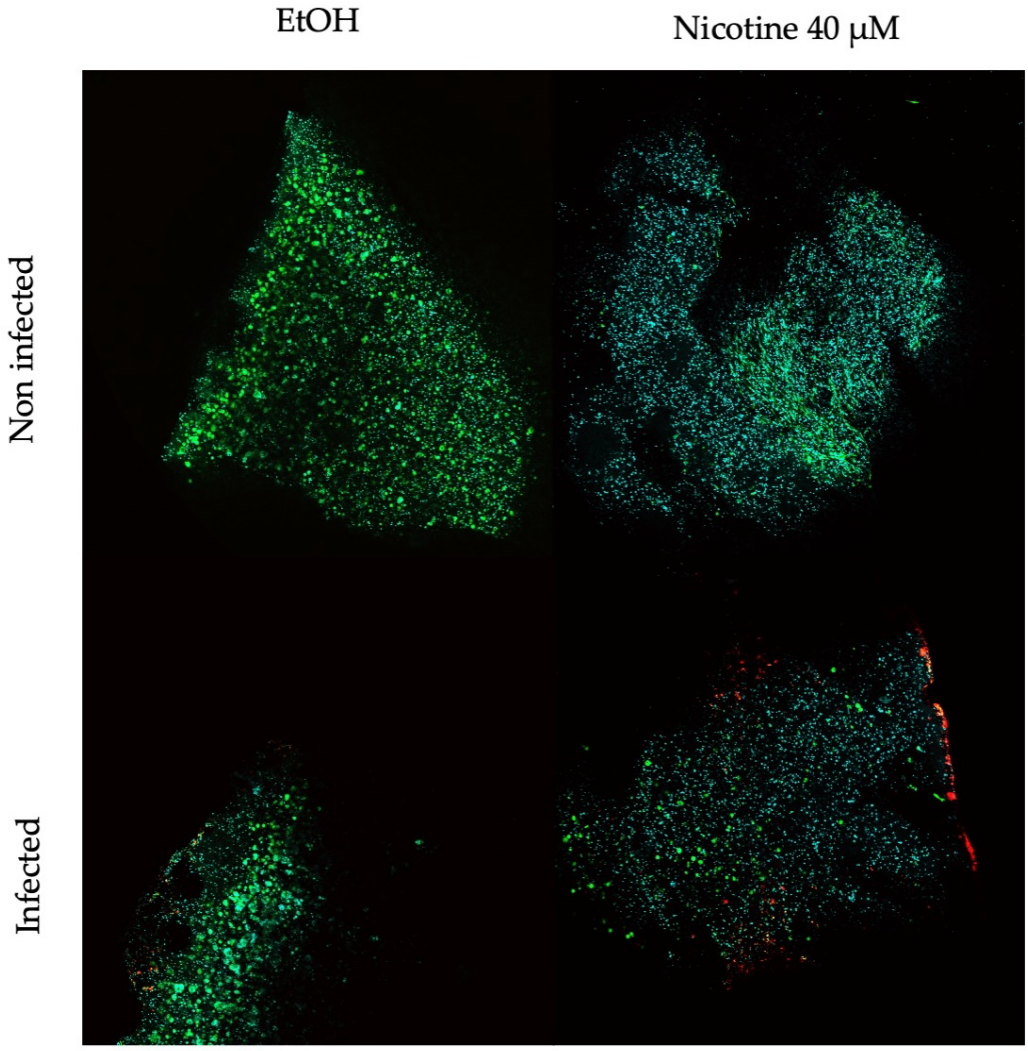

Figure 16. Distribution differences of Mtb H37Rv_mCHERRY (in red) and Calcein AM-stained cells (in green) within a 3D granuloma model analyzed via focal microscopy. Three days post-infection, the nicotine-treated model showed bacterial presence even in the central portion of the granuloma, whereas, in the ethanol-treated model, bacteria were predominantly trapped in the outer epithelial layer (granuloma shell), with very few in the center.

The CFU counts in the 3D model confirmed the effect of the nicotine treatment. In particular, they show significant differences between the control (EtOH) and nicotine (40 uM) treatment groups. Nicotine exposure increased CFU in the treated group compared to the control group, suggesting that nicotine may promote the growth and proliferation of Mtb (Figure 17).

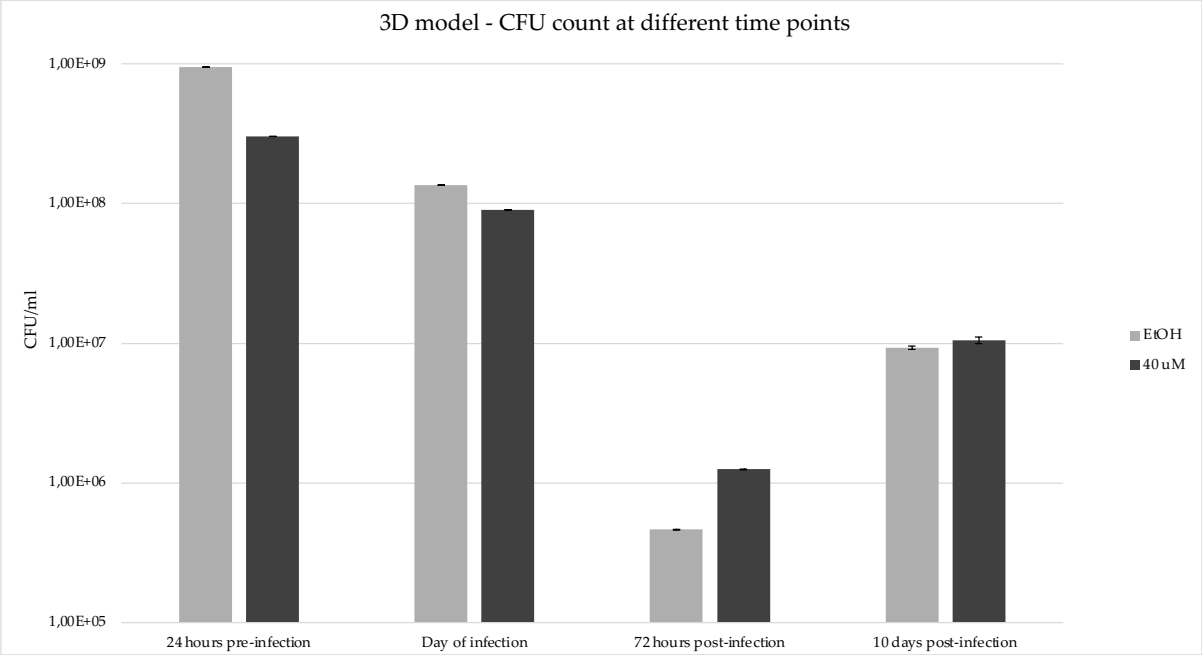

Figure 17. The graph represents the CFU counts in the 3D granuloma-like model composed of HBEC3-KT, hTERT-HLF, and THP-1 cells infected with Mtb H37Rv_mCHERRY. The chart shows CFU values at different time points (24 hours before the Mtb H37Rv_mCHERRY infection, the day of the infection, 72 hours post-infection, and 10 days after the infection) for the control (EtOH) and nicotine (40 uM) treatment groups. Nicotine exposure resulted in higher CFU counts at all time points than the control group. Data are presented as the mean CFU counts from

triplicate experiments. Data were normalized to inoculum (CFU counts set as 100%). The untreated control for the nicotine treatment consists of cells cultured in a standard medium supplemented with the highest ethanol (EtOH) concentration in the nicotine dilutions (40 μM). Values represent the mean ± standard deviation (SD) from at least three independent experiments. $p < 0.05$ indicates a statistically significant difference compared to the control.

Chapter 6: Discussion

This study represents a significant advancement in tuberculosis (TB) research. It leverages a three-dimensional (3D) bioprinted lung model to investigate the impact of nicotine-induced oxidative stress on Mtb infection.

Unlike conventional two-dimensional (2D) cultures and animal models, which present inherent limitations in replicating human lung microenvironments, this 3D bioprinted system offers unprecedented physiological accuracy in mimicking granuloma formation and host-pathogen interactions.

The novelty of this study lies in its ability to recreate the structural and cellular complexity of the pulmonary microenvironment with a fully humanized approach. Traditional 2D cultures fail to capture the spatial architecture and dynamic interactions of lung cells, while animal models suffer from interspecies differences in immune responses despite their contributions to TB research. This study overcomes these challenges by developing a model that incorporates human bronchial epithelial cells, lung fibroblasts, and macrophages and allows precise control over experimental conditions. This innovative model provides deeper insights into the role of oxidative stress, particularly nicotine exposure, in compromising epithelial barrier integrity and enhancing *Mycobacterium Tuberculosis* (Mtb) infection susceptibility. Moreover, this 3D bioprinted model aligns with the principles of the 3Rs—Replacement, Reduction, and Refinement—by reducing reliance on animal experimentation and offering a more ethical and sustainable alternative. The ability to simulate the human lung microenvironment with high fidelity makes this platform a transformative tool for TB research, with potential applications extending beyond this study.

The well-established association between cigarette smoke (CS) exposure and an increased risk of TB is supported by several epidemiological evidence. However, the specific role of nicotine, a key component of CS, in influencing immune function remains less thoroughly characterized.

This issue is particularly pressing given the rising prevalence of smokeless nicotine products, such as electronic cigarettes, nicotine pouches, and other alternatives marketed as safer than conventional cigarettes. With millions of individuals globally turning to these products, understanding how nicotine exposure affects immune responses to TB has become increasingly important [14].

Given the absence of an established biological model that fully recapitulates the complexity of nicotine's impact on Mtb infection within the human respiratory system, this study aimed to assess the effects of nicotine exposure on Mtb infection using a cellular model composed of lung fibroblasts (LF-hTERT), bronchial epithelial cells (HBEC-3kt), and monocytes (THP-1). This approach may offer a new framework for investigating the complex interactions between cellular components—lung fibroblasts, bronchial epithelial cells, and macrophages/monocytes—the infective pathogen Mtb and the role of an exogenous substance like nicotine. Moreover, the use of 3D bioprinted models in this study not only enhances the physiological relevance of in vitro systems but also addresses critical limitations seen in traditional models. Unlike 2D cultures, which lack spatial and mechanical cues, the 3D bioprinted models provide a dynamic and interactive microenvironment that closely resembles *in vivo* lung tissue. Furthermore, these models outperform animal systems by allowing direct observation of human-specific immune responses and granuloma dynamics, thereby reducing interspecies variability. The integration of multiple cell types into a structured model enables a comprehensive analysis of the interaction

among epithelial, immune, and stromal cells under oxidative stress and nicotine exposure. This methodological advancement represents a significant step forward in TB research, offering a powerful tool for mechanistic research and developing targeted therapies interventions.

Nicotine exposure affects cell viability across all cell types, particularly at 24 hours post-exposure. This observation aligns with previous studies demonstrating that CS components impair lung cell function through oxidative stress and apoptosis [83]. Notably, the observed reduction in cell viability appeared to diminish with prolonged incubation, suggesting that nicotine's impact is more likely due to impaired cellular metabolism, characteristic of oxidative stress induction, rather than direct cytotoxic effects. Oxidative stress leads to DNA damage, genomic instability, and DNA hypomethylation during short-term exposure, while prolonged exposure may result in apoptosis resistance and increased growth rate. Nicotine-induced ROS can act as signal transducers, influencing key regulatory pathways, including NF-κB activation. Although studies on nicotine's toxicity yield contradictory results, its role in ROS generation and NF-κB activation highlights its potential to disrupt cellular homeostasis, contributing to pathogenesis and toxicity [84]. This underscores the need for further investigation into nicotine’s mechanisms of action and its broader implications for human health.

The literature shows that immune cells are sensitive to nicotine-induced oxidative stress [85]. This is important to consider since impaired immune cell function may hinder the formation of effective granulomas, a key defense mechanism in TB. This may facilitate increased bacterial replication and accelerate disease progression. These results underscore the detrimental impact of nicotine on TB outcomes and emphasize the need for targeted interventions to preserve immune cell function in individuals exposed to CS [86].

Indeed, we focused part of our study on differentiated THP-1 cells. Macrophages were historically classified into two distinct subtypes based on their activation status: M1, characterized by pro-inflammatory properties, and M2, associated with anti-inflammatory and tissue repair functions. However, this binary classification is now regarded as an oversimplification of macrophage phenotypes' highly dynamic and heterogeneous nature. Due to the lack of better options, we decided to use the classical classification.

M1 macrophages, or classically activated macrophages, are primarily induced by interferon-gamma (IFN-γ) and lipopolysaccharides (LPS). These macrophages exhibit robust pro-inflammatory activity, producing high levels of ROS, nitric oxide (NO), and pro-inflammatory cytokines like tumor necrosis factor-alpha (TNF-α) and interleukin-12 (IL-12). These factors enhance the host's ability to control Mtb by promoting phagocytosis and destroying intracellular bacteria. However, excessive M1 responses can lead to tissue damage due to inflammation [87].

In contrast, M2 macrophages, a subset of alternatively activated macrophages, are induced by interleukins such as IL-4 and IL-13. These cells are characterized by anti-inflammatory properties and are involved in tissue repair and immune regulation. During MTB infection, M2 macrophages contribute to creating a more permissive environment for bacterial survival by dampening the inflammatory response and reducing the production of bactericidal molecules like NO. This phenotype can facilitate Mtb persistence and immune evasion, promoting latent or chronic infection and the tissue homeostasis required to contain the infection.

In our experimental settings, nicotine was observed to facilitate bacterial infection in M2 macrophages. Despite a significant reduction in macrophage survival, this did not correlate with decreased intracellular mycobacterial levels.

This suggests that the bacterial burden was relatively higher in nicotine-treated wells than in controls, as evidenced by comparable CFU/ml counts under reduced host cell viability. Interestingly, nicotine appeared to have minimal impact on M1 macrophages, highlighting a differential effect that warrants further investigation [13]. Ongoing studies aim to elucidate this selective response's mechanisms, including potential differences in nicotine metabolism, receptor expression, or resistance to oxidative stress between macrophage subtypes [88].

While most studies have primarily focused on the immune system's role, the surrounding pulmonary microenvironment has often been overlooked. At the same time, emerging evidence highlights the importance of epithelial barrier integrity in maintaining lung health and function. Therefore, it is critical to investigate the effects of nicotine on these “neglected” components of the lung [89,90]. The interactions between immune cells, the epithelial barrier, and the broader pulmonary microenvironment are fundamental in shaping the host response to Mtb infection. Elucidating how nicotine modulates these interactions may offer new insights into the mechanisms through which smoking exacerbates TB progression and identify potential therapeutic targets for mitigating its harmful effects on lung health.

The integrity of the lung's epithelial barrier is predominantly maintained by tight junctions (TJs) between lung epithelial cells, which regulate paracellular permeability and the selective passage of molecules [12]. These junctions consist of key proteins such as claudins, occludin, junctional adhesion molecules (JAMs), and Zonula Occludens (ZO) proteins [91]. Among these, claudin-1, occludin, and ZO-1 are particularly susceptible to oxidative stress. Nicotine, a well-known oxidative stressor, has been shown to alter the expression and subcellular localization of these TJ proteins, thereby compromising epithelial barrier

integrity. This disruption increases lung permeability, possibly facilitating pathogen invasion and exacerbating the inflammatory response during Mtb infection [92–94].

Bronchial epithelial cells, as the first line of defense against inhaled pathogens, play a critical role in the initial immune response to Mtb. These cells not only form the physical barrier but also interact with immune components, contributing to the establishment of the pulmonary microenvironment. Nicotine's ability to compromise TJ integrity and its immunomodulatory effects can impair the epithelial barrier's function, increasing susceptibility to Mtb infection [95]. The disruption of TJs weakens the epithelial cells' capacity to form an effective physical barrier, which may alter immune signaling pathways and further enhance the risk of infection and inflammation [96].

In the context of Mtb infection, the loss of tight junction integrity provides a route for pathogen translocation, allowing Mtb to breach the epithelial barrier more easily. Additionally, the altered immune signaling resulting from nicotine exposure can modify the response to infection, leading to an enhanced inflammatory environment conducive to Mtb growth and dissemination. This dual impact—on both the epithelial and immune responses—emphasizes the importance of understanding the full scope of nicotine's effects on pulmonary defenses. Therefore, elucidating the mechanisms by which nicotine affects epithelial and immune cell function is essential for developing targeted interventions to mitigate the detrimental effects of smoking on tuberculosis progression and improve therapeutic strategies for smokers affected by the disease.

Lung fibroblasts play a pivotal role in tissue repair and immune cell recruitment during TB infection. Our findings indicate that nicotine exposure significantly reduces fibroblast viability and bacterial load, suggesting that it

may impair fibroblast function and hinder Mtb replication. This observation aligns with previous reports indicating that fibroblasts can serve as reservoirs for Mtb during chronic infections, and their functional impairment may influence bacterial persistence and tissue remodeling [97]. Reduced fibroblast activity may compromise the host's ability to maintain tissue integrity and coordinate immune responses, further exacerbating disease progression.

Inflammation plays a dual role in TB, serving as a vital defense mechanism while also contributing to tissue damage and disease progression. Our findings indicate that nicotine modulates the inflammatory response in a cell-type-specific manner. While nicotine exposure may promote inflammasome activation and enhance bacterial clearance in monocytes, it may also exacerbate oxidative stress and inflammatory damage, as reported in prior studies [83]. In contrast, epithelial cells, which play a key role in orchestrating the pulmonary immune response, may become less efficient in recruiting and activating immune cells under nicotine exposure. This could facilitate Mtb persistence in the lung microenvironment. The complex interplay between nicotine, oxidative stress, and inflammation requires further investigation, particularly in the context of TB progression in smokers and individuals exposed to second-hand smoke.

Our study highlights the need to consider environmental factors, such as nicotine exposure, when investigating TB pathogenesis and developing management strategies: future research should focus on the molecular mechanisms underlying nicotine's effects on immune cell function, inflammasome activation, and epithelial-immune cell interactions. Additionally, investigating the impact of nicotine on lung-resident memory T cells, which are critical for long-term immunity against TB, could provide valuable insights into the development of targeted interventions [97].

Most of the previously described results from this thesis or other research papers have been produced using classical 2D cultures. While these models have been instrumental in demonstrating the direct effects of nicotine on lung fibroblasts, bronchial epithelial cells, and THP-1 monocytes, they provide a limited representation of the complex pulmonary microenvironment during Mtb infection[89].

In 2D cultures, each cell type is isolated from the dynamic interactions that occur *in vivo* between epithelial cells, immune cells, and fibroblasts. This isolation may overlook critical aspects of cellular crosstalk, extracellular matrix (ECM) signaling, and spatial organization, which are essential for accurately modeling the host response to environmental stressors and pathogens [88,98].

Developing and using 3D co-culture systems, which incorporate multiple lung cell types in a more physiologically relevant architecture, can address these limitations. Such systems facilitate direct cell-cell and cell-ECM interactions, better mimicking the lung's structural and functional complexity. Three-dimensional models can replicate the formation of granulomas, a hallmark of TB infection, and provide a platform to investigate how nicotine exposure influences individual cell behavior and the collective response of the pulmonary microenvironment.

To overcome the limitations of traditional 2D culture systems, we developed a granuloma-like model using 3D bioprinting technology. This model integrates human bronchial epithelial cells (HBEC3-KT), lung fibroblasts (hTERT-HLF), and THP-1-derived macrophages organized into a core-shell structure. The outer shell, consisting of HBECs embedded in CELLINK Bioink, mimics the epithelial barrier. At the same time, the core, composed of fibroblasts and differentiated macrophages within CELLINK Laminink 411, simulates the

immune microenvironment characteristic of granulomatous structures observed in tuberculosis (TB).

The bioprinted construct, with precise dimensions of 4 × 4 × 4 mm and an inner core of 2 × 2 × 2 mm, was fabricated using the CELLINK Bio X 3D bioprinter [99]. The model underwent dual crosslinking through ultraviolet (UV) and ionic stabilization processes to ensure structural stability and optimal cell viability. This 3D co-culture system provides a more physiologically relevant environment than traditional 2D cultures, enabling direct interactions between epithelial, mesenchymal, and immune cells. The three-dimensional configuration facilitates the formation of granuloma-like structures, closely resembling *in vivo* conditions during Mtb infection. Furthermore, it allows for a more accurate investigation of ROS dynamics and their impact on TJ integrity. ROS production varies across cellular compartments, influencing localized oxidative stress levels and disrupting the epithelial barrier.

In 3D models, oxidative stress in epithelial cells can propagate to neighboring fibroblasts and immune cells through paracrine signaling, amplifying tissue damage and inflammation [94]. This highlights the importance of intercellular communication in breaking the epithelial barrier and disseminating Mtb across lung tissue. Additionally, the 3D co-culture system provides a versatile platform for testing potential therapeutic interventions to mitigate oxidative stress and restore TJ integrity. Antioxidants and other agents targeting ROS-mediated damage can be evaluated for their efficacy in preserving epithelial barrier function and preventing Mtb invasion.

Overall, this 3D granuloma-like model offers a more comprehensive and physiologically relevant approach to studying nicotine's impact on tuberculosis progression. It facilitates deeper insights into the interactions between

environmental stressors, host immune responses, and bacterial persistence in the lung microenvironment.

Our preliminary findings indicate that nicotine exposure within this 3D model affects both epithelial and immune components, compromising barrier integrity and altering macrophage function. Notably, the granuloma-like structure provides a platform to investigate how environmental stressors, such as nicotine, modulate the interplay between epithelial and immune cells in a more realistic context. This approach highlights the importance of transitioning from 2D to 3D systems to better understand the pathophysiology of TB, particularly in smokers and individuals exposed to second-hand smoke [11,100].

Future studies utilizing this 3D model could further elucidate the molecular mechanisms by which nicotine influences TB progression, including its impact on cytokine signaling, oxidative stress responses, and bacterial clearance. Additionally, the model can be adapted to incorporate other cell types, such as lung-resident memory T cells, to explore their role in long-term immunity and identify potential therapeutic targets to mitigate the detrimental effects of smoking on TB outcomes.

The use of human lung organoids to model Mtb infection represents a significant advancement in in vitro research [16]. This model more accurately reflects human pathology than traditional two-dimensional cell cultures or animal models. Integrating lung epithelial cells and macrophages in these organoids enables studying host-pathogen interactions in a complex, dynamic environment.

Notably, Mtb infection in human lung organoids demonstrates how Mtb can infect both epithelial cells and macrophages, replicating the initial stages of tuberculosis infection. Furthermore, this model facilitates long-term culture, allowing the researchers to monitor the persistence of Mtb inside the organoids

across several passages. The potential of using hLOs extends to evaluating host-directed therapies (HDTs), such as the knockdown of MFN2 and HERPUD1, which were shown to reduce Mtb survival and inflammatory cytokine production within the organoids [101].

In the context of your study, integrating the effects of nicotine on TJ integrity and immune responses could be explored further using this advanced model. Combining human lung organoids with immune cells would provide valuable insights into how nicotine may exacerbate Mtb infection by disrupting the epithelial barrier and immune functions, leading to more effective host-directed therapeutic strategies.

Chapter 7: Conclusions

This study examined the effects of nicotine exposure on Mtb infection using a 3D-printed model comprising lung fibroblasts (LF-hTERT), bronchial epithelial cells (HBEC-3kt), and monocytes (THP-1). The findings demonstrate that nicotine accelerated bacterial uptake by epithelial cells despite having minimal direct effects on each cell type. This altered the infection dynamics and facilitated bacterial invasion. These observations suggest that nicotine enhances Mtb's ability to invade and persist within host cells.

The use of a three-dimensional (3D) model in this study is particularly significant, as it more closely mimics the natural microenvironment of the lung compared to traditional two-dimensional (2D) cultures. The 3D model allows for a more accurate simulation of cell-cell interactions and tissue architecture, providing a more physiologically relevant context for studying host-pathogen dynamics. This approach enabled us to properly understand nicotine's mechanism of action and, more in general, enhanced the reliability and translational potential of the findings, offering a more comprehensive understanding of how nicotine influences TB infection. Our results also reveal the significant role of oxidative stress in disrupting TJ integrity and impairing epithelial barrier function. Future studies should focus on further quantifying oxidative damage, particularly investigating the oxidation and degradation of key TJ proteins in 3D lung models exposed to nicotine and Mtb.

Despite these insights, the precise mechanisms by which nicotine modulates epithelial cell susceptibility to bacterial uptake remain unclear and warrant further investigation. Elucidating these pathways is essential for understanding how smoking-related compounds contribute to the progression of tuberculosis (TB).

Exploring antioxidant therapies and evaluating the efficacy of ROS-scavenging agents could offer promising solutions for restoring TJ integrity and enhancing barrier function, thereby improving the host's defense against Mtb. Moreover, understanding the molecular pathways involved in ROS-mediated TJ disruption will provide essential insights into potential therapeutic targets for preserving epithelial barrier integrity.

Integrating advanced models, such as 3D lung organoids, offers a promising approach to studying these complex interactions in a more physiologically relevant context. These models provide an opportunity to test host-directed therapies that target oxidative stress and preserve lung barrier function, ultimately contributing to more effective strategies for combating tuberculosis, particularly in populations at high risk due to chronic nicotine exposure.

The broader implications of this research emphasize the urgent need to address the infection-promoting and immunosuppressive effects of nicotine, particularly considering the increasing global use of smokeless nicotine products. These findings underscore the importance of integrating this knowledge into public health strategies and TB management programs to mitigate the disease burden associated with both smoking and alternative nicotine consumption.

Chapter 8: Methodological Limitations and Considerations

While the development of the 3D bioprinted lung model represents a significant advancement over traditional 2D cultures and animal models, several challenges emerged during its optimization. Addressing these issues required iterative adjustments in bio-ink composition and printing parameters, highlighting the need for more standardized protocols in 3D bioprinting.

The initial experiments underscored the need to optimize the protocol, which led to several key modifications to improve the consistency and relevance of the results.

Scaffold Material and Biocompatibility

The choice of bioink and hydrogel composition played a crucial role in maintaining cell viability and mimicking physiological conditions. However, achieving an optimal balance between scaffold rigidity and cellular permeability was challenging. Stiffer scaffolds provided better structural integrity but sometimes limited cell migration and interaction, whereas softer scaffolds were more permissive but risked structural collapse over time.

Cellular Integration and Distribution

The model aimed to replicate the lung's cellular complexity by integrating epithelial cells, fibroblasts, and immune components. However, ensuring uniform cell distribution within the 3D scaffold remained a challenge. In particular, macrophages exhibited varying migration patterns, which could influence granuloma formation dynamics. Future iterations of this model may incorporate microfluidic systems or perfusion bioreactors to improve cellular organization and dynamic interactions.

Oxygen and Nutrient Diffusion

Oxygen gradients play a crucial role in granuloma formation and Mtb dormancy, yet replicating these conditions in vitro posed technical difficulties. The static culture system may not fully mimic hypoxic regions found in TB granulomas *in vivo*. Future refinements could integrate oxygen-controlled bioreactors or engineered oxygen-releasing biomaterials to create more physiologically relevant conditions.

Long-Term Stability and Repeatability

Another key consideration was the reproducibility of infection dynamics in the 3D model. While the model successfully demonstrated Mtb colonization and granuloma-like formation, maintaining its stability over extended culture periods was challenging. Factors such as hydrogel degradation, bacterial overgrowth, and cellular senescence introduced variability, suggesting a need for further optimization of culture conditions.

Comparability to *In Vivo* Conditions

Although this model offers a more physiologically relevant platform than 2D cultures, it still lacks certain *in vivo* features, such as the full complexity of the immune system and lung biomechanics. To improve translational relevance, future adaptations might incorporate air-liquid interface models, immune cell recruitment systems, or vascularized microenvironments.

Structural Challenges and Knowledge Gaps

A comprehensive understanding of the three-dimensional structure of human granulomas remains incomplete, particularly regarding standardized parameters such as shape and thickness, given the inherent heterogeneity of their internal organization. This knowledge gap constrains the ability to develop

accurate in vitro models and limits the potential applications of 3D bioprinting in this context. However, the extent to which these structural parameters influence granuloma function and infection dynamics remains uncertain, as mechanobiological studies are currently lacking. In this study, we designed a granuloma-mimetic structure composed of a central core of monocytes/macrophages, supported by resident connective cells, and encapsulated by an epithelial layer, thereby partially replicating a simplified lung-like environment. To investigate bacterial infiltration and infection dynamics, we exposed the model to a bacterial suspension in the presence or absence of nicotine, a factor hypothesized to enhance bacterial uptake and facilitate infection establishment. Notably, the initial cellular composition of our model already reflected an inflamed phenotype, a critical consideration for the interpretation of infection dynamics within this system.

Other Limitations

Additionally, while this study focuses on structural lung cells like fibroblasts and epithelial cells, the direct impact of nicotine on other cell types involved in Mtb infection, such as dendritic cells and T lymphocytes, remains unexplored. Immune cell responses to nicotine-induced oxidative stress could alter the overall pathogenesis of Mtb infection. Studies addressing the broader immune landscape in the context of chronic nicotine exposure would be valuable for a more comprehensive understanding of the host-pathogen interactions.

Another limitation is using only one strain of Mtb (H37Rv), which may not fully capture the variability in infection dynamics, especially considering that it only partially represents linage-like strains and that Mtb lineages present substantial differences in fitness and infection capability. Moreover, the effects of nicotine on the infection and immune response in the context of multidrug-

resistant or extensively drug-resistant (MDR/XDR) Mtb strains could differ, and further research involving different Mtb strains is needed to assess the broader implications of nicotine exposure on tuberculosis progression.

Finally, the study primarily investigates the acute effects of nicotine exposure. The long-term effects of chronic nicotine use, particularly in the context of prolonged infection, remain unknown. Chronic exposure to nicotine may induce alterations in lung tissue that could modify the host's response to Mtb over time, potentially complicating the disease progression. Longitudinal studies examining the cumulative effects of nicotine exposure on both the epithelial barrier and immune responses in chronic infection models are essential for understanding its role in tuberculosis outcomes.

Future Directions

To overcome these limitations, future studies could focus on developing perfused lung-on-chip systems to better replicate oxygen gradients and cellular interactions. Moreover, it is essential to work on incorporating additional immune components to enhance granuloma modeling, including dendritic cells and T-cell subpopulations and on refining bio-ink compositions to imprint, although physiologically relevant, in vitro models such as 2D and 3D cultures can only partially replicate the complexity of the human pulmonary microenvironment. While 3D lung models, including organoids, offer significant advantages in simulating tissue architecture and host-pathogen interactions, they still lack the complete representation of systemic immune responses and other physiological factors in a living organism.

Acknowledgments

I wish to express my deepest gratitude to all those who have supported me along the way.

First and foremost, I would like to thank my supervisor, Professor Rita Rezzani, for her guidance and presence. Her expertise and passion for research have been a constant source of inspiration.

A heartfelt thank you also goes to the research group members in Brescia for their support and collaboration, which made this journey more stimulating and enriching.

I am particularly grateful to the Emerging Bacterial Pathogens group at the TB Supranational Reference Laboratory in IRCCS San Raffaele Scientific Institute, where this thesis has been partially carried out.

I sincerely thank Professor Daniela Maria Cirillo and the entire team for their warm welcome, guidance, and the opportunity to conduct part of my research in such a dynamic and stimulating environment.

A special thank you goes to Dr. Paolo Miotto, particularly to Dr. Andrea Muscetti and Dr. Bazezew Yenew, whose invaluable support and presence were fundamental throughout the laboratory work.

In the end, my greatest thanks go to Dr. Sorrentino (without whom this thesis would not even have a title) for her continuous support and invaluable assistance throughout these months.

Last but not least, I want to thank all those who believed in me during these years, even when I struggled to believe in myself.

Thank you to those who stayed, even through the most challenging moments, "*whatever it takes*".

References

1. Vazquez-Armendariz, A.I.; Tata, P.R. Recent Advances in Lung Organoid Development and Applications in Disease Modeling. *Journal of Clinical Investigation* **2023**, *133*, doi:10.1172/JCI170500.

2. Kühl, L.; Graichen, P.; von Daacke, N.; Mende, A.; Wygrecka, M.; Potaczek, D.P.; Miethe, S.; Garn, H. Human Lung Organoids—A Novel Experimental and Precision Medicine Approach. *Cells* **2023**, *12*.

3. Salgueiro, L.; Kummer, S.; Sonntag-Buck, V.; Weiß, A.; Schneider, M.A.; Kräusslich, H.-G.; Sotillo, R. Generation of Human Lung Organoid Cultures from Healthy and Tumor Tissue to Study Infectious Diseases. *J Virol* **2022**, *96*, doi:10.1128/jvi.00098-22.

4. Corleis, B.; Bastian, M.; Hoffmann, D.; Beer, M.; Dorhoi, A. Animal Models for COVID-19 and Tuberculosis. *Front Immunol* **2023**, *14*.

5. Yang, H.J.; Wang, D.; Wen, X.; Weiner, D.M.; Via, L.E. One Size Fits All? Not in In Vivo Modeling of Tuberculosis Chemotherapeutics. *Front Cell Infect Microbiol* **2021**, *11*.

6. Flynn, J.L.; Chan, J.; Lin, P.L. Macrophages and Control of Granulomatous Inflammation in Tuberculosis. *Mucosal Immunol* **2011**, *4*, 271–278.

7. Cadena, A.M.; Fortune, S.M.; Flynn, J.L. Heterogeneity in Tuberculosis. *Nat Rev Immunol* **2017**, *17*, 691–702.

8. Guirado, E.; Schlesinger, L.S. Modeling the Mycobacterium Tuberculosis Granuloma - the Critical Battlefield in Host Immunity and Disease. *Front Immunol* **2013**, *4*, doi:10.3389/fimmu.2013.00098.

9. Dorhoi, A.; Kaufmann, S.H.E. Tumor Necrosis Factor Alpha in Mycobacterial Infection. *Semin Immunol* **2014**, *26*, 203–209, doi:10.1016/j.smim.2014.04.003.

10. Kang, G.Y.; Rhyu, H.J.; Choi, H.H.; Shin, S.J.; Hyun, Y.M. 3D Imaging of the Transparent Mycobacterium Tuberculosis-Infected Lung Verifies the Localization of Innate Immune Cells With Granuloma. *Front Cell Infect Microbiol* **2020**, *10*, doi:10.3389/fcimb.2020.00226.

11. Miramontes, C.V.; Rodríguez-Carlos, A.; Marin-Luévano, S.P.; Trejo Martínez, L.A.; de Haro Acosta, J.; Enciso-Moreno, J.A.; Rivas-Santiago, B. Nicotine Promotes the Intracellular Growth of Mycobacterium Tuberculosis in Epithelial Cells. *Tuberculosis* **2021**, *127*, doi:10.1016/j.tube.2020.102026.

12. Wittekindt, O.H. Tight Junctions in Pulmonary Epithelia during Lung Inflammation. *Pflugers Arch* **2017**, *469*, 135–147.

13. Bai, X.; Stitzel, J.A.; Bai, A.; Zambrano, C.A.; Phillips, M.; Marrack, P.; Chan, E.D. Nicotine Impairs Macrophage Control of Mycobacterium Tuberculosis. *Am J Respir Cell Mol Biol* **2017**, *57*, 324–333, doi:10.1165/rcmb.2016-0270OC.

14. Cipollina, C.; Bruno, A.; Fasola, S.; Cristaldi, M.; Patella, B.; Inguanta, R.; Vilasi, A.; Aiello, G.; Grutta, S. La; Torino, C.; et al. Cellular and Molecular Signatures of Oxidative Stress in Bronchial Epithelial Cell Models Injured by Cigarette Smoke Extract. *Int J Mol Sci* **2022**, *23*.

15. Warburton, D.; Schwarz, M.; Tefft, D.; Flores-Delgado, G.; Anderson, K.D.; Cardoso, W. V *The Molecular Basis of Lung Morphogenesis*;

16. Archer, F.; Bobet-Erny, A.; Gomes, M. State of the Art on Lung Organoids in Mammals. *Vet Res* **2021**, *52*.

17. Deprez, M.; Zaragosi, L.E.; Truchi, M.; Becavin, C.; García, S.R.; Arguel, M.J.; Plaisant, M.; Magnone, V.; Lebrigand, K.; Abelanet, S.; et al. A Single-Cell Atlas of the Human Healthy Airways. *Am J Respir Crit Care Med* **2020**, *202*, 1636–1645, doi:10.1164/rccm.201911-2199OC.

18. Dichtl, S.; Posch, W.; Wilflingseder, D. The Breathtaking World of Human Respiratory in Vitro Models: Investigating Lung Diseases and Infections in 3D Models, Organoids, and Lung-on-Chip. *Eur J Immunol* **2024**, *54*.

19. World Health Assembly Global Strategy and Targets for Tuberculosis Prevention, Care and Control after 2015 (Resolution WHA67.1, Agenda Item 12.1). .

20. Corleis, B.; Bastian, M.; Hoffmann, D.; Beer, M.; Dorhoi, A. Animal Models for COVID-19 and Tuberculosis. *Front Immunol* **2023**, *14*.

21. Fitzgerald, L.E.; Abendaño, N.; Juste, R.A.; Alonso-Hearn, M. Three-Dimensional in Vitro Models of Granuloma to Study Bacteria-Host Interactions, Drug-Susceptibility, and Resuscitation of Dormant Mycobacteria. *Biomed Res Int* **2014**, *2014*.

22. Sustainable Development Goals .

23. Houben, R.M.G.J.; Dodd, P.J. The Global Burden of Latent Tuberculosis Infection: A Re-Estimation Using Mathematical Modelling. *PLoS Med* **2016**, *13*, doi:10.1371/journal.pmed.1002152.

24. Mahmoudi, S.; García, M.J.; Drain, P.K. Current Approaches for Diagnosis of Subclinical Pulmonary Tuberculosis, Clinical Implications and Future Perspectives: A Scoping Review. *Expert Rev Clin Immunol* **2024**, *20*, 715–726.

25. Drain, P.K.; Bajema, K.L.; Dowdy, D.; Dheda, K.; Naidoo, K.; Schumacher, S.G.; Ma, S.; Meermeier, E.; Lewinsohn, D.M.; Sherman, D.R. *Incipient and Subclinical Tuberculosis: A Clinical Review of Early Stages and Progression of Infection*; **2018**;

26. Migliori, G.B.; Ong, C.W.M.; Petrone, L.; D'ambrosio, L.; Centis, R.; Goletti, D. The Definition of Tuberculosis Infection Based on the Spectrum of Tuberculosis Disease. *Breathe* **2021**, *17*.

27. Delogu, G.; Sali, M.; Fadda, G. The Biology of Mycobacterium Tuberculosis Infection. *Mediterr J Hematol Infect Dis* **2013**, *5*.

28. Swain, S.S.; Sharma, D.; Hussain, T.; Pati, S. Molecular Mechanisms of Underlying Genetic Factors and Associated Mutations for Drug Resistance in Mycobacterium Tuberculosis. *Emerg Microbes Infect* **2020**, *9*, 1651–1663.

29. Gimenes Lima, G.; Portilho, A.I.; De Gaspari, E. Animal Models to Test SARS-CoV-2 Vaccines: Which Ones Are in Use and Future Expectations. *Pathogens* **2023**, *12*.

30. Rydell-Törmänen, K.; Johnson, J.R. The Applicability of Mouse Models to the Study of Human Disease. In *Methods in Molecular Biology*; Humana Press Inc., **2019**; Vol. 1940, pp. 3–22.

31. Harrison, D.E.; Astle, C.M.; Niazi, M.K.K.; Major, S.; Beamer, G.L. Genetically Diverse Mice Are Novel and Valuable Models of Age-Associated Susceptibility to Mycobacterium Tuberculosis. *Immunity and Ageing* **2014**, *11*, doi:10.1186/s12979-014-0024-6.

32. Kurtz, S.L.; Rossi, A.P.; Beamer, G.L.; Gatti, D.M.; Kramnik, I.; Elkins, K.L. The Diversity Outbred Mouse Population Is an Improved Animal Model of Vaccination against Tuberculosis That Reflects Heterogeneity of Protection. *mSphere* **2020**, *5*, doi:10.1128/msphere.00097-20.

33. Singhal, A.; Aliouat, E.M.; Hervé, M.; Mathys, V.; Kiass, M.; Creusy, C.; Delaire, B.; Tsenova, L.; Fleurisse, L.; Bertout, J.; et al. Experimental Tuberculosis in the Wistar Rat: A Model for Protective Immunity and Control of Infection. *PLoS One* **2011**, *6*, doi:10.1371/journal.pone.0018632.

34. Sugawara, I.; Yamada, H.; Mizuno, S. Pathological and Immunological Profiles of Rat Tuberculosis. *Int J Exp Pathol* **2004**, *85*, 125–134, doi:10.1111/j.0959-9673.2004.00379.x.

35. Turner, O.C.; Basaraba, R.J.; Orme, I.M. Immunopathogenesis of Pulmonary Granulomas in the Guinea Pig after Infection with *Mycobacterium Tuberculosis*. *Infect Immun* **2003**, *71*, 864–871, doi:10.1128/IAI.71.2.864-871.2003.

36. Dharmadhikari, A.S.; Nardell, E.A. What Animal Models Teach Humans about Tuberculosis. *Am J Respir Cell Mol Biol* **2008**, *39*, 503–508.

37. Subbian, S.; Tsenova, L.; O'Brien, P.; Yang, G.; Kushner, N.L.; Parsons, S.; Peixoto, B.; Fallows, D.; Kaplan, G. Spontaneous Latency in a Rabbit Model of Pulmonary Tuberculosis. *Am J Pathol* **2012**, *181*, 1711–1724, doi:10.1016/j.ajpath.2012.07.019.

38. Blanc, L.; Sarathy, J.P.; Cabrera, N.A.; O'Brien, P.; Dias-Freedman, I.; Mina, M.; Sacchettini, J.; Savic, R.M.; Gengenbacher, M.; Podell, B.K.; et al. Impact of Immunopathology on the Antituberculous Activity of Pyrazinamide. *Journal of Experimental Medicine* **2018**, *215*, 1975–1986, doi:10.1084/jem.20180518.

39. Rifat, D.; Prideaux, B.; Savic, R.M.; Urbanowski, M.E.; Parsons, T.L.; Luna, B.; Marzinke, M.A.; Ordonez, A.A.; DeMarco, V.P.; Jain, S.K.; et al. Pharmacokinetics of Rifapentine and Rifampin in a Rabbit Model of Tuberculosis and Correlation with Clinical Trial Data. *Sci Transl Med* **2018**, *10*, doi:10.1126/scitranslmed.aai7786.

40. Peña, J.C.; Ho, W.-Z. Monkey Models of Tuberculosis: Lessons Learned. *Infect Immun* **2015**, *83*, 852–862, doi:10.1128/IAI.02850-14.

41. Michelitsch, A.; Wernike, K.; Ulrich, L.; Mettenleiter, T.C.; Beer, M. SARS-CoV-2 in Animals: From Potential Hosts to Animal Models. In; **2021**; pp. 59–102.

42. Weiss, G.; Schaible, U.E. Macrophage Defense Mechanisms against Intracellular Bacteria. *Immunol Rev* **2015**, *264*, 182–203, doi:10.1111/imr.12266.

43. Meurens, F.; Summerfield, A.; Nauwynck, H.; Saif, L.; Gerdts, V. The Pig: A Model for Human Infectious Diseases. *Trends Microbiol* **2012**, *20*, 50–57, doi:10.1016/j.tim.2011.11.002.

44. Tannenbaum, J.; Bennett, B.T. Russell and Burch's 3Rs Then and Now: The Need for Clarity in Definition and Purpose. *J Am Assoc Lab Anim Sci* **2015**, *54*, 120–132.

45. Rodriguez Perez, C.; Shaw, D.M.; Earp, B.D.; Elger, B.S.; Persson, K. One R or the Other – an Experimental Bioethics Approach to 3R Dilemmas in Animal Research. *Med Health Care Philos* **2024**, *27*, 497–512, doi:10.1007/s11019-024-10221-y.

46. Travaglini, K.J.; Nabhan, A.N.; Penland, L.; Sinha, R.; Gillich, A.; Sit, R. V.; Chang, S.; Conley, S.D.; Mori, Y.; Seita, J.; et al. A Molecular Cell Atlas of the Human Lung from Single-Cell RNA Sequencing. *Nature* **2020**, *587*, 619–625, doi:10.1038/s41586-020-2922-4.

47. Posch, W.; Vosper, J.; Noureen, A.; Zaderer, V.; Witting, C.; Bertacchi, G.; Gstir, R.; Filipek, P.A.; Bonn, G.K.; Huber, L.A.; et al. C5aR Inhibition of Nonimmune Cells Suppresses Inflammation and Maintains Epithelial Integrity in SARS-CoV-2–Infected Primary Human Airway Epithelia. *Journal of Allergy and Clinical Immunology* **2021**, *147*, 2083-2097.e6, doi:10.1016/j.jaci.2021.03.038.

48. Kim, M.; Mun, H.; Sung, C.O.; Cho, E.J.; Jeon, H.J.; Chun, S.M.; Jung, D.J.; Shin, T.H.; Jeong, G.S.; Kim, D.K.; et al. Patient-Derived Lung Cancer Organoids as in Vitro Cancer Models for Therapeutic Screening. *Nat Commun* **2019**, *10*, doi:10.1038/s41467-019-11867-6.

49. Dijkstra, K.K.; Monkhorst, K.; Schipper, L.J.; Hartemink, K.J.; Smit, E.F.; Kaing, S.; de Groot, R.; Wolkers, M.C.; Clevers, H.; Cuppen, E.; et al. Challenges in Establishing Pure Lung Cancer Organoids Limit Their Utility for Personalized Medicine. *Cell Rep* **2020**, *31*, doi:10.1016/j.celrep.2020.107588.

50. Tindle, C.; Fuller, M.; Fonseca, A.; Taheri, S.; Ibeawuchi, S.-R.; Beutler, N.; Dattatray Katkar, G.; Claire, A.; Castillo, V.; Hernandez, M.; et al. Adult Stem Cell-Derived Complete Lung Organoid Models Emulate Lung Disease in COVID-19. **2021**, *0*, 66417, doi:10.7554/eLife.

51. Lamers, M.M.; Mykytyn, A.Z.; Breugem, T.I.; Wang, Y.; Wu, D.C.; Riesebosch, S.; van den Doel, P.B.; Schipper, D.; Bestebroer, T.; Wu, N.C.; et al. Human Airway Cells Prevent Sars-Cov-2 Multibasic Cleavage Site Cell Culture Adaptation. *Elife* **2021**, *10*, doi:10.7554/ELIFE.66815.

52. Low, L.A.; Mummery, C.; Berridge, B.R.; Austin, C.P.; Tagle, D.A. Organs-on-Chips: Into the next Decade. *Nat Rev Drug Discov* 2021, *20*, 345–361.

53. Shen, C.; Yang, H.; She, W.; Meng, Q. A Microfluidic Lung-on-a-Chip Based on Biomimetic Hydrogel Membrane. *Biotechnol Bioeng* **2023**, *120*, 2027–2038, doi:10.1002/bit.28426.

54. Van Riet, S.; Van Schadewijk, A.; De Vos, S.; Vandeghinste, N.; Rottier, R.J.; Stolk, J.; Hiemstra, P.S.; Khedoe, P. Modulation of Airway Epithelial Innate Immunity and Wound Repair by M(GM-CSF) and M(M-CSF) Macrophages. *J Innate Immun* **2020**, *12*, 410–421, doi:10.1159/000506833.

55. Bordoni, V.; Matusali, G.; Mariotti, D.; Antonioli, M.; Cimini, E.; Sacchi, A.; Tartaglia, E.; Casetti, R.; Grassi, G.; Notari, S.; et al. The Interplay between SARS-CoV-2 Infected Airway Epithelium and Immune Cells Modulates Regulatory/Inflammatory Signals. *iScience* **2022**, *25*, doi:10.1016/j.isci.2022.103854.

56. van der Vaart, J.; Lamers, M.M.; Haagmans, B.L.; Clevers, H. Advancing Lung Organoids for COVID-19 Research. *DMM Disease Models and Mechanisms* 2021, *14*.

57. Kumar, V.; Varghese, S. Ex Vivo Tumor-on-a-Chip Platforms to Study Intercellular Interactions within the Tumor Microenvironment. *Adv Healthc Mater* **2019**, *8*.

58. Elkington, P.; Lerm, M.; Kapoor, N.; Mahon, R.; Pienaar, E.; Huh, D.; Kaushal, D.; Schlesinger, L.S. In Vitro Granuloma Models of Tuberculosis: Potential and Challenges. *Journal of Infectious Diseases* **2019**, *219*, 1858–1866.

59. Daniel, J.; Deb, C.; Dubey, V.S.; Sirakova, T.D.; Abomoelak, B.; Morbidoni, H.R.; Kolattukudy, P.E. Induction of a Novel Class of Diacylglycerol Acyltransferases and Triacylglycerol Accumulation in Mycobacterium Tuberculosis as It Goes into a Dormancy-like State in Culture. *J Bacteriol* **2004**, *186*, 5017–5030, doi:10.1128/JB.186.15.5017-5030.2004.

60. Parasa, V.R.; Rahman, M.J.; Hoang, A.T.N.; Svensson, M.; Brighenti, S.; Lerm, M. Modeling Mycobacterium Tuberculosis Early Granuloma Formation in Experimental Human Lung Tissue. *DMM Disease Models and Mechanisms* **2014**, *7*, 281–288, doi:10.1242/dmm.013854.

61. Via, L.E.; Schimel, D.; Weiner, D.M.; Dartois, V.; Dayao, E.; Cai, Y.; Yoon, Y.S.; Dreher, M.R.; Kastenmayer, R.J.; Laymon, C.M.; et al. Infection Dynamics and Response to Chemotherapy in a Rabbit Model of Tuberculosis Using [18F]2-Fluoro-Deoxy-D-Glucose Positron Emission Tomography and Computed Tomography. *Antimicrob Agents Chemother* **2012**, *56*, 4391–4402, doi:10.1128/AAC.00531-12.

62. Workman, V.L.; Tezera, L.B.; Elkington, P.T.; Jayasinghe, S.N. Controlled Generation of Microspheres Incorporating Extracellular Matrix Fibrils for Three-Dimensional Cell Culture. *Adv Funct Mater* **2014**, *24*, 2648–2657, doi:10.1002/adfm.201303891.

63. Bielecka, M.K.; Tezera, L.B.; Zmijan, R.; Drobniewski, F.; Zhang, X.; Jayasinghe, S.; Elkington, P. A Bioengineered Three-Dimensional Cell Culture Platform Integrated with Microfluidics to Address Antimicrobial Resistance in Tuberculosis. *mBio* **2017**, *8*, doi:10.1128/mBio.02073-16.

64. Cantin, A.M.; North, S.L.; Fells, G.A.; Hubbard, R.C.; Crystal, R.G. *Oxidant-Mediated Epithelial Cell Injury in Idiopathic Pulmonary Fibrosis*;

65. Rahman, I.; Adcock, I.M. Oxidative Stress and Redox Regulation of Lung Inflammation in COPD. *European Respiratory Journal* **2006**, *28*, 219–242, doi:10.1183/09031936.06.00053805.

66. Albano, G.D.; Gagliardo, R.P.; Montalbano, A.M.; Profita, M. Overview of the Mechanisms of Oxidative Stress: Impact in Inflammation of the Airway Diseases. *Antioxidants* 2022, *11*.

67. Rogers, L.K.; Cismowski, M.J. Oxidative Stress in the Lung – The Essential Paradox. *Curr Opin Toxicol* **2018**, *7*, 37–43.

68. Seo, Y.S.; Park, J.M.; Kim, J.H.; Lee, M.Y. Cigarette Smoke-Induced Reactive Oxygen Species Formation: A Concise Review. *Antioxidants* **2023**, *12*.

69. Bargagli, E.; Olivieri, C.; Bennett, D.; Prasse, A.; Muller-Quernheim, J.; Rottoli, P. Oxidative Stress in the Pathogenesis of Diffuse Lung Diseases: A Review. *Respir Med* **2009**, *103*, 1245–1256.

70. Kinnula, V.L.; Fattman, C.L.; Tan, R.J.; Oury, T.D. Oxidative Stress in Pulmonary Fibrosis: A Possible Role for Redox Modulatory Therapy. *Am J Respir Crit Care Med* 2005, *172*, 417–422.

71. Taylor, J.L.; Hattle, J.M.; Dreitz, S.A.; Troudt, J.L.M.; Izzo, L.S.; Basaraba, R.J.; Orme, I.M.; Matrisian, L.M.; Izzo, A.A. Role for Matrix Metalloproteinase 9 in Granuloma Formation during Pulmonary Mycobacterium Tuberculosis Infection. *Infect Immun* **2006**, *74*, 6135–6144, doi:10.1128/IAI.02048-05.

72. Gain, C.; Song, S.; Angtuaco, T.; Satta, S.; Kelesidis, T. The Role of Oxidative Stress in the Pathogenesis of Infections with Coronaviruses. *Front Microbiol* **2023**, *13*.

73. Vidhya, R.; Rathnakumar, K.; Balu, V.; Pugalendi, K.V. Oxidative Stress, Antioxidant Status and Lipid Profile in Pulmonary Tuberculosis Patients before and after Anti-Tubercular Therapy. *Indian Journal of Tuberculosis* **2019**, *66*, 375–381, doi:10.1016/j.ijtb.2018.11.002.

74. Asikainen, T.M.; Raivio, K.O.; Saksela, M.; Kinnula, V.L. *Expression and Developmental Profile of Antioxidant Enzymes in Human Lung and Liver*; 1998; Vol. 19;.

75. Otterbein, L.E.; Choi, A.M.K. Heme Oxygenase: Colors of Defense against Cellular Stress. *American Journal of Physiology-Lung Cellular and Molecular Physiology* **2000**, *279*, L1029–L1037, doi:10.1152/ajplung.2000.279.6.L1029.

76. Tenhunen, R.; Marver, H.S.; Schmid, R. The Enzymatic Conversion of Heme to Bilirubin by Microsomal Heme Oxygenase. *Proceedings of the National Academy of Sciences* **1968**, *61*, 748–755, doi:10.1073/pnas.61.2.748.

77. Choi, A.M.; Alam, J. Heme Oxygenase-1: Function, Regulation, and Implication of a Novel Stress-Inducible Protein in Oxidant-Induced Lung Injury. *Am J Respir Cell Mol Biol* **1996**, *15*, 9–19, doi:10.1165/ajrcmb.15.1.8679227.

78. Maines, M.D. THE HEME OXYGENASE SYSTEM:A Regulator of Second Messenger Gases. *Annu Rev Pharmacol Toxicol* **1997**, *37*, 517–554, doi:10.1146/annurev.pharmtox.37.1.517.

79. Park, E.-M.; Park, Y.-M.; Gwak, Y.-S. Oxidative Damage in Tissues of Rats Exposed to Cigarette Smoke. *Free Radic Biol Med* **1998**, *25*, 79–86, doi:10.1016/S0891-5849(98)00041-0.

80. Leiva-Juárez, M.M.; Kolls, J.K.; Evans, S.E. Lung Epithelial Cells: Therapeutically Inducible Effectors of Antimicrobial Defense. *Mucosal Immunol* **2018**, *11*, 21–34, doi:10.1038/mi.2017.71.

81. Johnston, S.L.; Goldblatt, D.L.; Evans, S.E.; Tuvim, M.J.; Dickey, B.F. Airway Epithelial Innate Immunity. *Front Physiol* **2021**, *12*, doi:10.3389/fphys.2021.749077.

82. Pace, E.; Di Vincenzo, S.; Ferraro, M.; Lanata, L.; Scaglione, F. Role of Airway Epithelium in Viral Respiratory Infections: Can Carbocysteine Prevent or Mitigate Them? *Immunology* **2024**, *172*, 329–342.

83. Barclay, A.M.; Ninaber, D.K.; Limpens, R.W.A.L.; Walburg, K. V.; Bárcena, M.; Hiemstra, P.S.; Ottenhoff, T.H.M.; van der Does, A.M.; Joosten, S.A. Mycobacteria Develop Biofilms on Airway Epithelial Cells and Promote Mucosal Barrier Disruption. *iScience* **2024**, *27*, doi:10.1016/j.isci.2024.111063.

84. Barr, J.; Sharma, C.S.; Sarkar, S.; Wise, K.; Dong, L.; Periyakaruppan, A.; Ramesh, G.T. Nicotine Induces Oxidative Stress and Activates Nuclear Transcription Factor Kappa B in Rat Mesencephalic Cells. *Mol Cell Biochem* **2007**, *297*, 93–99, doi:10.1007/s11010-006-9333-1.

85. Theobald, S.J.; Müller, T.A.; Lange, D.; Keck, K.; Rybniker, J. The Role of Inflammasomes as Central Inflammatory Hubs in Mycobacterium Tuberculosis Infection. *Front Immunol* **2024**, *15*, doi:10.3389/fimmu.2024.1436676.

86. Cha, S.R.; Jang, J.; Park, S.M.; Ryu, S.M.; Cho, S.J.; Yang, S.R. Cigarette Smoke-Induced Respiratory Response: Insights into Cellular Processes and Biomarkers. *Antioxidants* **2023**, *12*.

87. Chan, E.D.; Bai, X. *Author Contribution Section and COI*;

88. Shastri, M.D.; Shukla, S.D.; Chong, W.C.; Dua, K.; Peterson, G.M.; Patel, R.P.; Hansbro, P.M.; Eri, R.; O'Toole, R.F. Role of Oxidative Stress in the Pathology and Management of Human Tuberculosis. *Oxid Med Cell Longev* **2018**, *2018*.

89. Wohnhaas, C.T.; Gindele, J.A.; Kiechle, T.; Shen, Y.; Leparc, G.G.; Stierstorfer, B.; Stahl, H.; Gantner, F.; Viollet, C.; Schymeinsky, J.; et al. Cigarette Smoke Specifically Affects Small Airway Epithelial Cell Populations and Triggers the Expansion of Inflammatory and Squamous Differentiation Associated Basal Cells. *International Journal of Molecular Sciences Article Int. J. Mol. Sci* **2021**, doi:10.3390/ijms.

90. Willemse, D.; Moodley, C.; Mehra, S.; Kaushal, D. Transcriptional Response of Mycobacterium Tuberculosis to Cigarette Smoke Condensate. *Front Microbiol* **2021**, *12*, doi:10.3389/fmicb.2021.744800.

91. Silva, S.; Bicker, J.; Falcão, A.; Fortuna, A. Air-Liquid Interface (ALI) Impact on Different Respiratory Cell Cultures. *European Journal of Pharmaceutics and Biopharmaceutics* **2023**, *184*, 62–82.

92. Birkness, K.A.; Deslauriers, M.; Bartlett, J.H.; White, E.H.; King, C.H.; Quinn, F.D. *An In Vitro Tissue Culture Bilayer Model To Examine Early Events in Mycobacterium Tuberculosis Infection*; **1999**; Vol. 67;.

93. Wang, Q.; Lucas, J.H.; Pang, C.; Zhao, R.; Rahman, I. Tobacco and Menthol Flavored Nicotine-Free Electronic Cigarettes Induced Inflammation and Dysregulated Repair in Lung Fibroblast and Epithelium. *Respir Res* **2024**, *25*, doi:10.1186/s12931-023-02537-9.

94. Tatsuta, M.; Kan-O, K.; Ishii, Y.; Yamamoto, N.; Ogawa, T.; Fukuyama, S.; Ogawa, A.; Fujita, A.; Nakanishi, Y.; Matsumoto, K. Effects of Cigarette Smoke on Barrier Function and Tight Junction Proteins in the Bronchial Epithelium: Protective Role of Cathelicidin LL-37. *Respir Res* **2019**, *20*, doi:10.1186/s12931-019-1226-4.

95. Htwe, S.S.; Harrington, H.; Knox, A.; Rose, F.; Aylott, J.; Haycock, J.W.; Ghaemmaghami, A.M. Investigating NF-KB Signaling in Lung Fibroblasts in 2D and 3D Culture Systems. *Respir Res* **2015**, *16*, doi:10.1186/s12931-015-0302-7.

96. Raduka, A.; Gao, N.; Chatburn, R.L.; Rezaee, F. Electronic Cigarette Exposure Disrupts Airway Epithelial Barrier Function and Exacerbates Viral Infection. *Am J Physiol Lung Cell Mol Physiol* **2023**, *325*, L580–L593, doi:10.1152/ajplung.00135.2023.

97. Perdomo, C.; Zedler, U.; Kühl, A.A.; Lozza, L.; Saikali, P.; Sander, L.E.; Vogelzang, A.; Kaufmann, S.H.E.; Kupz, A. Mucosal BCG Vaccination Induces Protective Lung-Resident Memory T Cell Populations against Tuberculosis. *mBio* **2016**, *7*, doi:10.1128/mBio.01686-16.

98. Kletting, S.; Barthold, S.; Repnik, U.; Griffiths, G.; Loretz, B.; Schneider-Daum, N.; de Souza Carvalho-Wodarz, C.; Lehr, C.M. Co-Culture of Human Alveolar Epithelial (HAELVi) and Macrophage (THP-1) Cell Lines. *ALTEX* **2018**, *35*, 211–222, doi:10.14573/altex.1607191.

99. Sbrana, F.V.; Pinos, R.; Barbaglio, F.; Ribezzi, D.; Scagnoli, F.; Scarfò, L.; Redwan, I.N.; Martinez, H.; Farè, S.; Ghia, P.; et al. 3D Bioprinting Allows the Establishment of Long-Term 3D Culture Model for Chronic Lymphocytic Leukemia Cells. *Front Immunol* **2021**, *12*, doi:10.3389/fimmu.2021.639572.

100. Braian, C.; Svensson, M.; Brighenti, S.; Lerm, M.; Parasa, V.R. A 3D Human Lung Tissue Model for Functional Studies on Mycobacterium Tuberculosis Infection. *Journal of Visualized Experiments* **2015**, *2015*, doi:10.3791/53084.

101. Kim, S.Y.; Choi, J.A.; Choi, S.; Kim, K.K.; Song, C.H.; Kim, E.M. Advances in an In Vitro Tuberculosis Infection Model Using Human Lung Organoids for Host-Directed Therapies. *PLoS Pathog* **2024**, *20*, doi:10.1371/journal.ppat.1012295.

Abbreviations:

- **2010/63/EU**: European Directive on Animal Welfare in Experiments (2010/63/EU)
- **22°C**: Standard Room Temperature (22 degrees Celsius)
- **2D**: Two-Dimensional Cell Culture
- **37°C**: Cell Incubation Temperature (37 degrees Celsius)
- **3D**: Three-Dimensional Cell Culture
- **3R**: "Replacement, Reduction, Refinement" (Ethical Principles for Animal Research)
- **4°C**: Refrigeration Temperature (4 degrees Celsius)
- **7H10**: Middlebrook Agar (Culture Medium for Mycobacteria)
- **7H10+10%**: Middlebrook Agar Supplemented with OADC (Oleic Acid-Albumin-Dextrose-Catalase)
- **7H9**: Middlebrook Broth (Liquid Medium for Mycobacteria Culture)
- **A549**: Human Alveolar Epithelial Cell Line
- **AB**: Antibiotic
- **ALI**: Air-Liquid Interface
- **AM**: Alveolar Macrophage
- **AT1**: Alveolar Type 1 Cells
- **AT2**: Alveolar Type 2 Cells
- **ATB**: Active Tuberculosis
- **ATCC®**: American Type Culture Collection
- **C**: Carbon (Chemical Element)
- **CAT**: Catalase (Antioxidant Enzyme)
- **CC**: Collaborative Cross (Mouse Genetic Lines for Research)
- **CD8**: Cluster of Differentiation 8 (Surface Protein of Cytotoxic T Cells)
- **CDK4**: Cyclin-Dependent Kinase 4
- **CELLINK**: Company Producing Bioink and 3D Bioprinters
- **CFU**: Colony-Forming Units
- **CHX**: Chlorhexidine
- **CM**: Cynomolgus Macaque
- **CO_2**: Carbon Dioxide

- **COPD**: Chronic Obstructive Pulmonary Disease
- **COVID-19**: Coronavirus Disease 2019
- **CS**: Cigarette Smoke
- **DLD**: Diffuse Lung Disease
- **DMEM/F12**: Dulbecco's Modified Eagle's Medium/Nutrient Mixture F-12
- **DNA**: Deoxyribonucleic Acid
- **DO**: Diversity Outbred (Genetically Diverse Mouse Line)
- **DPBS**: Dulbecco's Phosphate-Buffered Saline
- **ECM**: Extracellular Matrix
- **EDTA**: Ethylenediaminetetraacetic Acid
- **ERK**: Extracellular Signal-Regulated Kinase
- **ETZ**: Electron-Transparent Zone
- **FAD**: Flavin Adenine Dinucleotide
- **FBS**: Fetal Bovine Serum
- **FIJI**: Image Analysis Software Based on ImageJ
- **G418**: Genetic Antibiotic (Neomycin Analog)
- **GSH**: Glutathione (Antioxidant)
- **GSSG**: Glutathione Disulfide (Oxidized Glutathione)
- **GSSG/2GSH**: Ratio of Oxidized to Reduced Glutathione
- **HAE**: Human Airway Epithelial Cells
- **HBEC-3kt**: Immortalized Bronchial Cell Line
- **HBSS**: Hank's Balanced Salt Solution
- **HERPUD1**: Homocysteine-Induced ER Protein with Ubiquitin-Like Domain 1
- **HIV**: Human Immunodeficiency Virus
- **HLA**: Human Leukocyte Antigen
- **HLF**: Human Lung Fibroblast
- **H_2O_2**: Hydrogen Peroxide
- **IL-12**: Interleukin 12
- **IL-13**: Interleukin 13
- **IL-4**: Interleukin 4

- **IL-6**: Interleukin 6
- **IL-8**: Interleukin 8
- **IPF**: Idiopathic Pulmonary Fibrosis
- **IRCCS**: Scientific Institute for Research, Hospitalization, and Healthcare
- **JNK**: c-Jun N-terminal Kinase
- **KSFM**: Keratinocyte Serum-Free Medium
- **L5**: L5 Phage (Used in Mycobacterium Plasmids)
- **LIVE/DEAD®**: Cell Viability Assay
- **LL-37**: Human Antimicrobial Cathelicidin
- **LPS**: Lipopolysaccharide
- **LTBI**: Latent Tuberculosis Infection
- **M**: Molarity
- **M0**: Undifferentiated Macrophage Phenotype
- **M1**: Classically Activated Macrophages
- **M2**: Alternatively Activated Macrophages
- **MAPK**: Mitogen-Activated Protein Kinase
- **MDR/RR-TB**: Multidrug-Resistant/Rifampicin-Resistant Tuberculosis
- **MDR/XDR**: Multidrug-Resistant/Extensively Drug-Resistant
- **MFN2**: Mitofusin 2
- **MMP-7**: Matrilysin (a Metalloproteinase)
- **MOI**: Multiplicity of Infection
- **MTB**: Mycobacterium Tuberculosis
- **MTBC**: Mycobacterium Tuberculosis Complex
- **NAD**: Nicotinamide Adenine Dinucleotide
- **NAD(P)H**: Reduced Form of NAD or NADP
- **NADPH**: Nicotinamide Adenine Dinucleotide Phosphate
- **NHP**: Non-Human Primate
- **NIC**: Nicotine
- **NK**: Natural Killer Cells
- **NO**: Nitric Oxide

- **OADC**: Oleic Acid-Albumin-Dextrose-Catalase
- **OADC+**: Culture Medium Enriched with OADC
- **OD**: Optical Density
- **OD_{600}**: Optical Density at 600 nm
- **$O_2\bullet^-$**: Superoxide Anion
- **PBS**: Phosphate-Buffered Saline
- **PCR**: Polymerase Chain Reaction
- **PMA**: Phorbol 12-Myristate 13-Acetate
- **R**: Resistance
- **RM**: Rhesus Macaque
- **RNS**: Reactive Nitrogen Species
- **ROS**: Reactive Oxygen Species
- **ROS/RNS**: Reactive Oxygen and Nitrogen Species
- **RPM**: Revolutions per Minute
- **RPMI**: Roswell Park Memorial Institute Medium
- **RS**: Reactive Species
- **S**: Sulfate
- **SAE**: Small Airway Epithelial Cells
- **SD**: Standard Deviation
- **SDS**: Sodium Dodecyl Sulfate
- **SM**: Medium Supplement
- **SOD**: Superoxide Dismutase
- **TB**: Tuberculosis
- **THP-1**: Human Monocytic Cell Line
- **TIB-202™**: ATCC Code for THP-1 Cell Line
- **TJ**: Tight Junction
- **UN**: United Nations
- **USA**: United States of America
- **UV**: Ultraviolet
- **V**: Volt

- **W**: Watt
- **WHO**: World Health Organization
- **X4**: Chemokine Receptor CXCR4
- **ZO**: Zona Occludens
- **ZO-1**: Zona Occludens 1
- **•OH**: Hydroxyl Radicals